Structure and Reactivity of 1,8-Bis(naphthalenediyl)dipnictanes.

Kevin Dzialkowski,[a] Alexander Gehlhaar,[a] Christoph Wölper,[a] Alexander A. Auer,[b] and Stephan Schulz*[a]

[a] Institute for Inorganic Chemistry and Center for Nanointegration Duisburg-Essen (Cenide), University of Duisburg-Essen, Universitätsstraße 5-7, D-45117 Essen, Germany.

[b] Max-Planck-Institut für Kohlenforschung, D-45470 Mülheim an der Ruhr, Germany

ABSTRACT: Syntheses and solid-state structures of diarsane $Naph_2As_2$ (Naph = 1,8-naphthalenediyl, **1**) and $(Naph)_5Sb_4Cl_2$ **3** are reported and the σ-donor capacity of $Naph_2E_2$ (E = As **1**, Sb **2**) was studied in reactions with $(coe)Cr(CO)_5$ (coe = *Z*-cyclooctene), yielding $Naph_2As_2[Cr(CO)_5]_2$ (**4**) and $Naph_2E_2Cr(CO)_5$ (E = As **5**, Sb **6**). In contrast, reactions of **1** and **3** with Me_2SAuCl proceed with oxidation and formation of elemental gold as well as $Naph_2(AsCl)_2$ (**7**) and $[NaphSbCl_2]_2$ **8**. All complexes were characterized by elemental analyses, heteronuclear (^1H, ^{13}C) NMR and FT-IR spectroscopy as well as single crystal X-ray diffraction. Intermolecular E···π interactions (E = As, Sb), which were observed in **7** and **8**, were quantified by use of density functional theory and local coupled cluster electronic structure theory calculations. These allow to assess the nature and relative importance of covalent and non-covalent interactions and illustrate how dispersion interactions change with the electronic structure of the series of compounds.

INTRODUCTION

Dipnictanes $R_2E\text{-}ER_2$ contain a central E-E bond and the group 15 elements adopt the oxidation state II. The first compound of this type, Me_4As_2, which is known as "*fuming arsenical liquid*" or "*Cacodyl*", was prepared by Louis Cadet de Gassicourt in 1760 and later on by Robert Bunsen,[1] whereas the heavier congeners Me_4Sb_2 and Me_4Bi_2 were prepared in the early 1930's.[2,3] Since distibanes and dibismuthanes exhibit rather weak Sb-Sb and Bi-Bi bonds,[4] they have been studied as promising starting reagents for the synthesis of persistent Sb- and Bi-centered radicals by thermally activated homolytic bond cleavage reactions.[5-7] In addition, some dipnictanes are thermochromic, which refers to the color change that occurs upon melting.[8-14] The thermochromic effect most likely results from the breakage of intermolecular metal···metal interactions, which exist in the solid state but disappear in the liquid state.[15-29]

Apart from the identification of attractive intermolecular interactions in such molecules, their coordination chemistry has also been studied. While diphosphanes R_4P_2 have been widely investigated, the heavier homologues have been studied to a far lesser extent and their capability to serve as ligands in main group metal and transition metal chemistry is still underdeveloped.[30] These findings clearly reflect the decreasing σ-donor capacity (Lewis basicity) of dipnictanes with increasing atomic number, which results from the increasing s-character of the electron lone pair.[31] Moreover, the weak E-E bond of the heaviest congeners limits the thermal stability of the complexes.

Our interest in the structure[32,33] and reactivity of dipnictanes R_4E_2 (E = Sb, Bi), which has led to the synthesis of group 13/15[34-38] and group 15/16 compounds,[39-41] prompted our attention to 1,8-naphthalenediyl-substituted (Naph) derivatives. *Peri*-substituted complexes of group 15 (type **I**)[42-47] and group 16 elements[48-52] as well as mixed group 15/16 compounds[53-56] are known (Scheme 1) and pnictogen-pnictogen as well as chalcogen-chalcogen interactions have been studied to some extent. Recently, we reported the synthesis of distibane $Naph_2Sb_2$ **2** (type **III**),[57] which was formed by reductive coupling of two Sb(III) centers as was observed in the reaction of 1,8-dilithionaphthalene $NaphLi_2$ with $PhPCl_2$, yielding $Naph(PPh)_2$ (type **II**).[58] The strength of intermolecular Sb···π interactions in the solid state of **2** was analyzed by dispersion-corrected quantum chemical calculations. These studies were expanded to the whole family of $Naph_2E_2$ (type **III**; E = P, As, Sb, Bi) and the results compared with the solid state structure of $Naph_2P_2$.[59] $Naph_2P_2$ showed intermolecular CH···π and π···π interactions but no P···π interactions. Based on electronic structure theory studies, we predicted similar structures for $Naph_2As_2$ **1** and $Naph_2P_2$, whereas $Naph_2Bi_2$ is expected to show intermolecular metal-π interactions as observed for $Naph_2Sb_2$ **2**.

Scheme 1. Structurally characterized 1,8-naphthalenediyl complexes of group 15 elements.

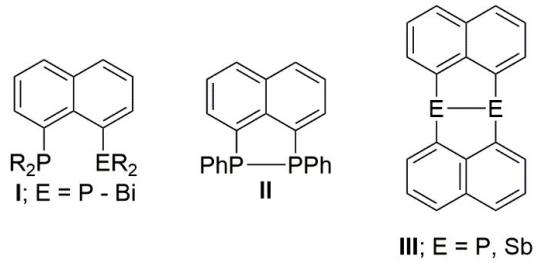

Interactions with π systems is well-known for trivalent pnictogen compounds[60-67] and pnictogen···π arene interactions in EX_3 (E = As, Sb, Bi, X = Cl, OCH_3, CH_3) adducts with benzene have recently been studied.[68] An analysis of the nature of the intermolecular interactions revealed the purely dispersive character (typically in the order of 10-20 kJ/mol) in case of weakly electron-accepting substituents, i.e. Me, whereas electron withdrawing substituents result in an increasing contribution of donor-acceptor π→σ* character and higher interaction energies of 30 kJ/mol for $AsCl_3$ and up to 60 kJ/mol for $BiCl_3$, respectively. Moreover, dipnictenes L(X)GaE=EGa(X)L were recently shown to exhibit dispersive pnicogen−π and H···H interactions between the organic ligands,[69] whereas a complex interplay between attractive dispersion and repulsive steric interactions was reported for *syn–syn* and *syn–anti* conformers of $Te(BiR_2)_2$.[70]

We herein report the syntheses and structures of $Naph_2As_2$ **1** and $Naph_5Sb_4Cl_2$ **3**, which was obtained from the reaction of $SbCl_3$

with $NaphLi_2$ in 4:5 molar ratio, whereas all attempts to synthesize $Naph_2Bi_2$ failed. Moreover, the σ-donor capacity of **1** and $Naph_2Sb_2$ **2** was studied in reactions with $coeCr(CO)_5$, yielding dinuclear $Naph_2As_2[Cr(CO)_5]_2$ **4** and mononuclear complexes $Naph_2Sb_2Cr(CO)_5$ (E = As **5**, Sb **6**), whereas oxidation reactions of **1** and **3** with Me_2SAuCl yielded $Naph_2(AsCl)_2$ **7** and $[NaphSbCl_2]_2$ **8**, respectively. The electronic structures of **1** to **8** were analyzed in detail by quantum chemical calculations.

RESULTS AND DISCUSSION

Synthesis and characterization. Reaction of $NaphLi_2$(TMEDA) with $AsCl_3$ in 3:2 molar ratio at –78 °C proceeded with elimination of LiCl and reduction of the arsenic center as was previously observed in the analogous reaction with $SbCl_3$ (Scheme 2).[57] Diarsane $Naph_2As_2$ **1** was obtained as light-orange crystalline solid in 52% yield, while perylene was identified by ^{1}H NMR spectroscopy.

Scheme 2. Syntheses of $Naph_2As_2$ 1.

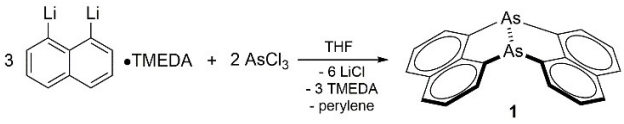

To optimize the yield of **2**, which often lacked from the difficulty of complete removal of coordinating TMEDA, we replaced $NaphLi_2$(TMEDA) by $NaphLi_2$, which was formed by reaction of 1,8-dibromonaphthalene with two equivalents of *n*-BuLi. Surprisingly, the reaction of $NaphLi_2$ with $SbCl_3$ in 3:2 molar ratio at –78 °C did not yield **2** but a rather complex reaction mixture, from which few crystals of $Naph_5Sb_4Cl_2$ (**3**) were isolated (Scheme 3). Repeating the reaction of $SbCl_3$ with $NaphLi_2$ in a 4:5 molar ratio gave $Naph_5Sb_4Cl_2$ (**3**) in 69% yield.

Scheme 3. Synthesis of $Naph_5Sb_4Cl_2$ 3.

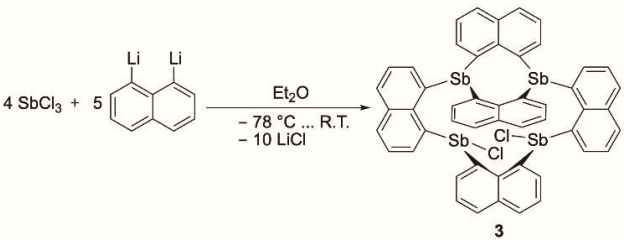

In contrast, any attempt to synthesize dibismuthane $Naph_2Bi_2$ by reaction of Li_2Naph(TMEDA) with either $BiCl_3$ or $BiBr_3$ at –78 °C in THF in a 3:2 molar ratio failed. Upon warming to ambient temperature, decomposition reactions with formation of elemental bismuth occurred. *In situ* ^{1}H-NMR studies at -78 °C on the reaction of $BiCl_3$ with Li_2Naph(TMEDA) showed the formation of a complex reaction mixture of various so far unidentified species, from which $Naph_2Bi_2$ could not be isolated even after workup at -78 °C. Reaction of this mixture with $coeCr(CO)_5$ did not result in the formation of $Naph_2Bi_2[Cr(CO)_5]$. Similar results were obtained by reacting Li_2Naph with $BiCl_3$ or $BiBr_3$ in 3:2 as well as 5:4 molar ratios.

1 and **3** were characterized by heteronuclear (^{1}H, ^{13}C) NMR spectroscopy (Table S1, S2). **1** is moderately soluble in toluene and $CHCl_3$. Its ^{1}H NMR spectrum shows two doublets (7.99, 7.63 ppm) and one triplet (7.40 ppm), which are only marginally shifted compared to the values reported for $Naph_2Sb_2$ **2** (doublets at 8.03 and 7.55 ppm, triplet at 7.34 ppm). The ^{13}C NMR spectrum of **1** also shows the expected six singlets for the Naph substituent (149.9, 141.4, 135.5, 131.3, 127.9, 126.9). **3** is poorly soluble in organic solvents and a ^{1}H NMR spectrum could only be recorded in a 5:1 mixture of toluene-d_8 and $CDCl_3$ at elevated temperature (70 °C). It shows four doublets (8.57, 8.08, 7.59 and 7.47 ppm) and one multiplet (7.41-7.34 ppm) in accordance with the lower symmetry of **3** compared to **2**. Due to the very low solubility of **3**, the ^{13}C NMR spectrum only shows signals of the solvent, even at elevated temperatures.

Single crystals of **1** were grown from a solution in $CHCl_3$. **1** crystallizes in the monoclinic space group $P2_1/c$ with four molecules in the unit cell (Figure 1). Selected bond lengths and angles are given in table 1.

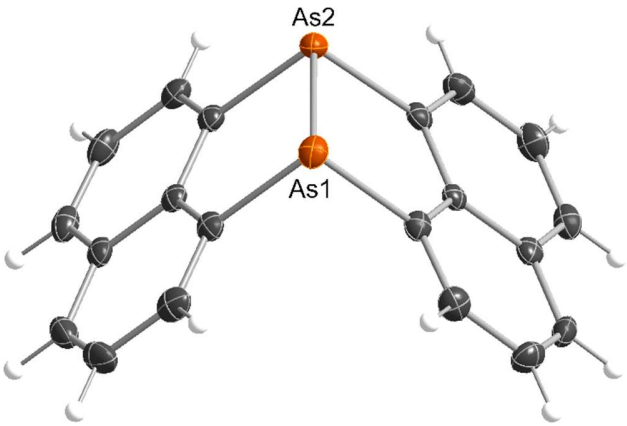

Figure 1. Molecular structure of 1 in the solid-state. Thermal ellipsoids are shown at the 50% probability level.

1 adopts a butterfly-type structure as was observed for $Naph_2Sb_2$ **2** with both arsenic atoms adopting trigonal-pyramidal coordination spheres. In accordance with the constrained geometry of **1**, the central As-As bond length (2.4326(4) Å) is at the lower end for As-As bond lengths reported for diarsanes,[71] but agrees with the sum of the single-bond covalent radii (As 1.19 Å).[62] The C-As-C (As1: 96.45(9)°; As2: 96.83(9)°) and C-As-As bond angles (As1: 90.82(7)°, 90.54(7)°; As2: 90.64(7)°, 90.92(7)°) are close to 90°, indicating a high p-orbital character of the bonding electrons. The sum of the C-E-C and C-E-E bond angles in $Naph_2As_2$ **1** are slightly larger compared to those observed in **2**, resulting in a larger bond angular sum in **1** (277.8°, 278.4°) compared to **2** (267.9°, 266.6°). The As-C bonds (1.961(2) – 1.964(2) Å) are within the typical range observed for As-C single bonds and agree well to the sum of the covalent radii (As 1.19 Å, C 0.73 Å).[72] The packing of the molecules within the crystal of **1** (Figure 2) differs from that observed for **2**. Intermolecular interactions in **1** are dominated brick-like, classical dispersion-dominated π···π and CH···π interactions of the Naph rings as was reported for $Naph_2P_2$,[59] whereas neither As···π nor As···As interactions were observed. These findings perfectly agree with our predictions from quantum chemical calculations.[57]

To rationalize and quantify the intermolecular interactions, DLPNO-CCSD(T)[73-78] calculations were performed for the series of $Naph_2As_2$, $Naph_2Sb_2$ and $Naph_2Bi_2$. The intermolecular by interactions in the dimer structures were analyzed using the Local Energy Decomposition (LED) method,[79,80] which allows to express the interaction energy in terms of geometric and electronic preparation, dispersive and non-dispersive contributions (Figure 3). The results are in good agreement with our previous

Table 1. Selected experimental [calculated][a] bond lengths [Å] and bond angles [°] of 1 - 3.

	1	**2**[55]	**3**
E-E[b]	2.4326(4) [2.468]	2.7972(3) [2.798]	3.0515(8)[c] [3.100], 3.1985(8) [3.128] 3.0468(8) [3.062]
E-C	1.961(2) [1.978] 1.963(2) [1.978] 1.961(2) [1.978] 1.964(2) [1.978]	2.1602(19) [2.176] 2.1695(18) [2.177] 2.1595(18) [2.176] 2.1658(19) [2.176]	2.179(9) [2.192], 2.205(9) [2.232] 2.141(9) [2.168], 2.144(9) [2.180] 2.134(8) [2.151], 2.138(9) [2.144] 2.186(9) [2.213], 2.206(9) [2.235]
Sb-Cl	-	-	2.535(2) [2.463], 2.5628(2) [2.463]
C-E-E	90.81(6) [90.4] 90.54(6) [90.1] 90.65(7) [90.1] 90.92(6) [90.4]	86.33(5) [86.3] 86.16(5) [86.1] 86.07(5) [86.3] 86.26(5) [86.5]	-
C-E-C	96.45(9) [95.7] 96.83(9) [95.7]	95.38(7) [93.2] 94.25(7) [93.2]	98.2(3) [96.5], 95.8(3) [94.6] 97.7(3) [96.4], 99.0(3) [101.2] 101.8(3) [98.5], 101.7(3) [104.2] 102.7(4) [100.8], 102.8(3) [102.7]

[a] Calculated at the BP86-D3/def2-TZVPP level of theory (def2-QZVP for E = As, Sb).[57] [b] E = As (**1**), Sb (**2**, **3**). [c] **3** doesn't show any Sb-Sb single bonds. The rather short distances result from the constrained geometry of the Naph substituents.

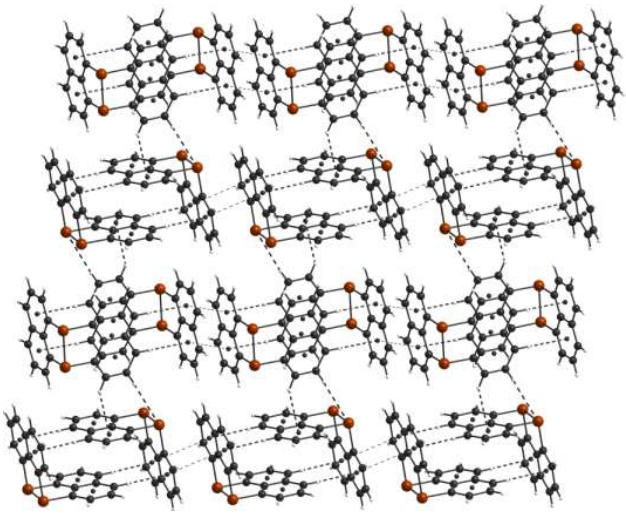

Figure 2. CH···π/π···π, CH···π and π···π interactions in the packing of 1 in the solid-state.

results obtained at the DFT-SAPT level of theory, proving that the dimers are mainly bound by dispersion interaction, which overcompensates the steric and electrostatic repulsion. This also explains the dominating π···π and CH···π interactions in the solid state structure, since pnictogen···π interactions are likely to be smaller in magnitude than the sum of other intermolecular interactions in this case. While the value of the D3 correction should be used merely as an indicator for the total dispersion contribution to the interaction energy, the relative values obtained at the BP86-D3 level of theory can be used to assess the importance of dispersion in intramolecular interactions.[79] LED and SAPT[57] values (in braces) show an increasing trend from As to Bi (As: –125 (–97, –100), Sb: –144 (–107, –101), Bi: –151 (–109, –105) kJ/mol). Note that the D3 correction for BP86 is larger by 30%, but roughly agrees with the observed trend. The total interaction energies show the expected trend (LED and SAPT in braces: As: –92 (–69) kJ/mol; Sb: –107 (–69, – 70) kJ/mol, Bi: –118.1 (–68.7, –69.1) kJ/mol).

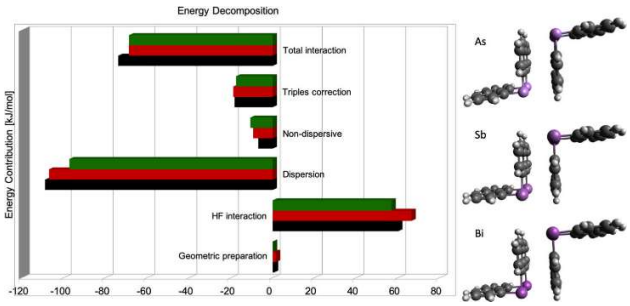

Figure 3. DLPNO-CCSD(T) LED-analysis of the Naph$_2$E$_2$ dimers (geometries optimized at the level BP86 def2/TZVPP of theory, DLPNO-CCSD(T)/cc-pVTZ using tight PNO settings). (bars in left panel - As: green, Sb: red and Bi: black).

Single crystals of **3** (Figure 4) were obtained from a solution in toluene/$CHCl_3$ (5:1). **3** crystallizes in the monoclinic space group $P2_1/n$ with four molecules in the unit cell and selected bond lengths and angles are given in table 1. **3** contains four Sb atoms in the oxidation state +3. Two Sb atoms (Sb2, Sb3) coordinate to three Naph substituents, whereas Sb1 and Sb4 are bound to two Naph ligands and one Cl atom. Sb-C bond lengths range from 2.134(8) to 2.206(9), and Sb-Cl bond lengths (2.535(2), 2.562(2) Å) are within the expected range. The bond angular sum at each Sb atom (Sb1 280.9(7)°, Sb2 301.2(9)°, Sb3 304.5(10)°, Sb4 282.5(7)°) is close to 270°, indicating a high p-orbital character of the bonding electrons. **3** shows rather short intramolecular Sb···Sb bond distances of 3.048, 3.055, 3.197 and 3.406 Å, respectively, which are far below the sum of the van der Waals radii (4.12 Å)[81] and most likely originate from the rigid molecular framework.

Intermolecular Sb···π interactions are not present (distance from centroid 3.634 and 4.502 Å) The Sb atoms are oriented towards a π-system, but the resulting Sb···π interaction is more likely a

side effect of a strong CH···Cl hydrogen bond rather than a determining factor of the packing (Figure S23), especially since the Naph ligand is oriented towards the Cl atom, resulting in a twisted conformation of the molecule.

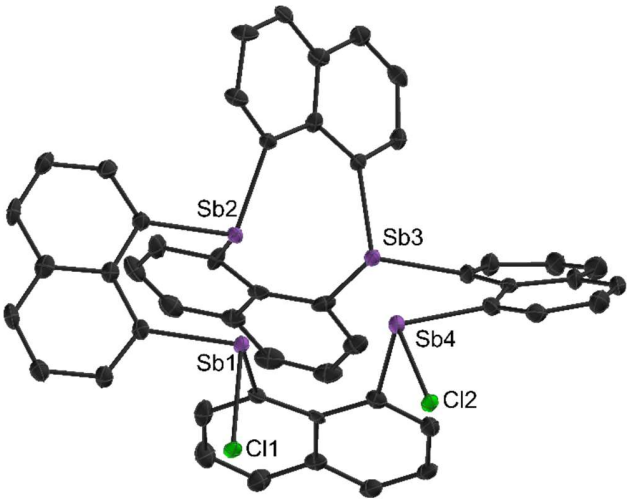

Figure 4. Molecular structure of 3 in the solid-state. Hydrogen atoms and co crystallized $CHCl_3$ were omitted for clarity. Thermal ellipsoids are shown at the 50% probability level.

σ-donor properties of $Naph_2E_2$

To study the σ-donor properties of **1** and **2** in coordination chemistry, we studied reactions with $coeCr(CO)_5$ (coe = *Z*-cyclooctene) in 1:2 molar ratio (Scheme 4). The reactions, which were accompanied by a color change from orange to yellow, proceeded with formation of cyclooctene as was proven by *in situ* ^{1}H NMR spectroscopy. However, while $coeCr(CO)_5$ was completely consumed in the reaction with **1**, indicating the formation of the binuclear complex $Naph_2As_2[Cr(CO)_5]_2$ **4**, only one equivalent of $coeCr(CO)_5$ was consumed in the reaction with **2** even after prolonged reaction time (24 h). The *in situ* ^{1}H NMR spectrum still showed one set of resonances of the coe ligand of $coeCr(CO)_5$ (5.63, 2.15 and 1.51 ppm). The attempted synthesis of the mononuclear complex $Naph_2As_2[Cr(CO)_5]$ by reaction of **1** with a sub-stoichiometric amount of $coeCr(CO)_5$ (1:0.9 molar ratio) gave a mixture of the mono- and binuclear complexes, which could not be separated by recrystallization. All crystallization experiment gave crystals with co-crystallized $Naph_2As_2[Cr(CO)_5]_2$ **4** and $Naph_2As_2[Cr(CO)_5]$ **5**, respectively.

Scheme 4. Complexation reaction of 1 and 2 with $(coe)Cr(CO)_5$.

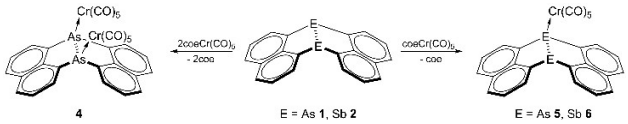

^{1}H and ^{13}C NMR spectra of $Naph_2As_2[Cr(CO)_5]_2$ **4** exhibit the expected resonances of the Naph ligands (Table S1, S2). The ^{13}C NMR spectrum shows two signals (221.1, 215.7 ppm) for the axial and equatorial carbonyl groups of the $Cr(CO)_5$ unit. The ^{1}H NMR spectrum shows two doublets (8.15 and 7.82 ppm) and one triplet at 7.59 ppm. Due to the asymmetrical substitution in $Naph_2Sb_2[Cr(CO)_5]$ **6**, the ^{1}H NMR spectrum of **6** shows two doublets of doublet (8.14, 7.82 ppm), one doublet of triplet (8.10 ppm) and one multiplet (7.75-7.42 ppm). The ^{13}C NMR spectrum of $Naph_2Sb_2[Cr(CO)_5]$ **6** shows the resonances of the Naph ligand (Table S2) as well as two signals (217.3, 216.3 ppm) due to the axial and equatorial carbonyl groups of the $Cr(CO)_5$ unit. The ^{1}H NMR spectrum of co-crystallized **4** and **5** shows two doublets at 8.17 and 7.85 ppm and one triplet at 7.55 ppm, which were assigned to **4**, and additional resonances at 8.11, 8.05, 7.75, 7.64 and 7.49 ppm, respectively, which were assigned to **5**.

Assuming an ideal C_{4v} symmetry of the $M(CO)_5$ fragment in **4** - **6**, three carbonyl absorptions corresponding to two A_1 and one E vibrational modes should be observed. In addition, the IR forbidden B_1 fundamental stretching is often observed as weak band in the IR spectra of such $Cr(CO)_5$ complexes as a result of the perturbation of the ideal C_{4v} symmetry as was reported for pnictinidene complexes $(ArE)Cr(CO)_5$ (E = As, Sb, Bi),[82] $H_3SbCr(CO)_5$,[83] $Ph_3ECr(CO)_5$ (E = As, Sb, Bi)[84] and other complexes of the general type $LCr(CO)_5$.[85-87] However, IR spectra of crystalline **4** - **6** are rather broad and contain more than the expected number of bands in the expected region of 1860–2060 cm^{-1} (Figures S9, S13, S16). Two sets of absorption bands due to the symmetrical and/or asymmetrical stretching vibration of the trans- and cis-oriented CO groups were found in the IR spectra of **4** (2064, 1992, 1910 cm^{-1}) and **6** (2070, 2057, 1999, 1991, 1942 cm^{-1}). Comparable findings were reported previously for pnictinidene complexes $(ArE)Cr(CO)_5$ (E = As, Sb, Bi), and these were attributed to a coupling of the carbonyl frequencies and the crystal splitting of the bands in the solid state.[82] Compared to the CO absorption band in $Cr(CO)_6$ (2000 cm^{-1}), a slight shift of the *transoid* CO band to higher wavenumbers is observed for **4** and **6**, indicating a weaker π-acceptor character of the Naph ligand compared to CO, resulting in a stronger π-backdonation into the CO acceptor orbital. On the other hand, a σ-donation was interpreted from the decreased wavenumbers of the equatorial CO groups in the square-pyramidal $Cr(CO)_5$ fragment (**4**: 1910 cm^{-1}; **6**: 1942 cm^{-1}) compared to 1965 cm^{-1} in $Cr(CO)_6$).[88] The experimental findings agree with the computed normal mode frequencies (**4'**: 2061, 1989, 1936 cm^{-1}; **6'**: 2049, 1978, 1956, 1942 cm^{-1}). The IR spectrum of co-crystallized **4** and **5** show a similar series of IR bands due to the symmetrical and/or asymmetrical stretching vibration of trans- and cis-oriented CO groups (2072, 2061, 1985, 1907 cm^{-1}), which could not be addressed to **4** and **5**. Computed IR spectra are given in the electronic supplement (Figures S39 - S35).

We also recorded IR spectra of **4** and **6** in $CDCl_3$ solution (Figures S10, S17), which show the A^{ax}_1 (**4**: 2064 cm^{-1}; **6**: 2066 cm^{-1}) and A^{eq}_1 absorption bands (**4**: 1949 cm^{-1}; **6**: 1946 cm^{-1}) due to the stretch of the axial and equatorial CO groups bonded in the *trans*- and cis-positions,[89] whereas we did not observe any B_1 stretching bands. In contrast, the A^{ax}_1 stretching frequencies of $(ArE)Cr(CO)_5$ (E = As, Sb, Bi; ~1894 cm^{-1} in CH_2Cl_2)[82] and $Ph_3ECr(CO)_5$ complexes (E = As, Sb, Bi; ~1949 cm^{-1})[84] are shifted to lower wave numbers, indicating that $Naph_2As_2$ and $Naph_2Sb_2$ are weaker electron donors compared to ArE and Ph_3E, respectively. The frequencies of the A^{ax}_1 wavelength in $Cr(CO)_5$ complexes of a polarized phosphaalkene (~1870 cm^{-1}),[90] or in carbene–phosphinidene adduct (~1865 cm^{-1})[91] are also shifted to lower wave numbers.

Single crystals of **4**, **5** and **6** were obtained from solutions in $CHCl_3$ (**4**), $CHCl_3$ (**5**) and CH_3CN (**6**). **4** and **6** crystallize in the triclinic space group *P*-1 with two molecules in the unit cell (Figures 5, 7), whereas **5** crystallizes in the monoclinic space

group $P2_1/n$ (Figure 6) with four molecules in the unit cell. Selected bond lengths and angles are given in Table 2.

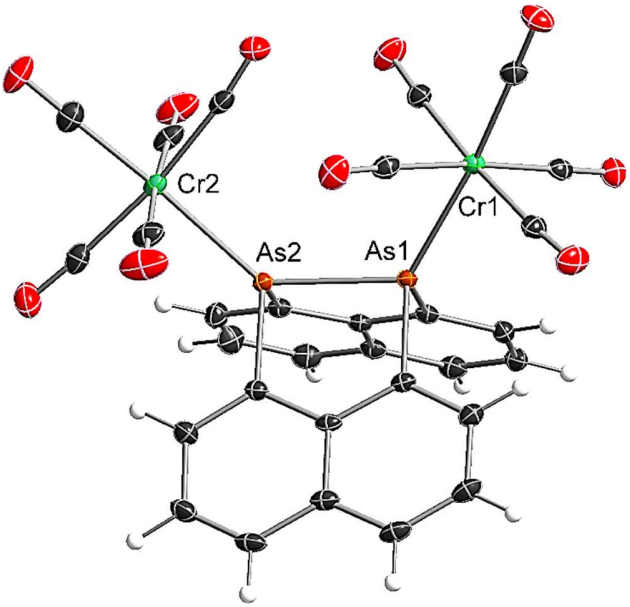

Figure 5. Molecular structure of 4 in the solid-state. Thermal ellipsoids are shown at the 50% probability level.

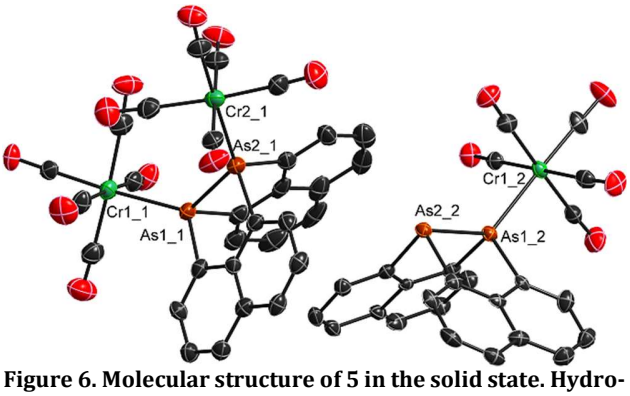

Figure 6. Molecular structure of 5 in the solid state. Hydrogen atoms and co-crystallized solvent (CH_3CN) were omitted for clarity. Thermal ellipsoids shown at the 50% probability level.

The As-As bond length in **4** (2.4248(3) Å) and **5** (2.4324(11) Å) are identical to that of **1** (2.4326(4) Å). The As-C bond lengths in **4** (1.9366(15), 1.9428(16), 1.9430(16), 1.9548(16) Å) and **5**, which marginally differ for threefold- (1.942(8), 1.947(8) Å) and fourfold- coordinated As atoms (1.954(8) Å, 1.965(8) Å), are slightly shorter compared to **1**, whereas the sum of the C-As-C and C-As-As bond angles in **4** (283.0°, 284.5°) are larger than in **1** (277.8°, 266.57(17)°). The bond angular sum of the pyramidal As atom (273.7°) in **5** is smaller compared to that of the fourfold-coordinated one (287.7°). The As-Cr bond lengths (**4**: 2.4402(3) Å, 2.4687(4) Å; **5**: 2.4726(15) Å) are comparable to that of $[Mes^*As{=}As(CH(SiMe_3)_2]Cr(CO)_5$ (2.454(1) Å).[92] In contrast, the Sb-Sb bond length decreases upon complexation (**6**: 2.7516(5) Å; **2**: 2.7972(3) Å) despite the increase in the coordination number, which typically results in a bond length elongation as was observed for instance for distibane adducts with group 13 trialkyls.[93,94] The shortening of the Sb-Sb bond in **6** points to an increasing p-orbital character of the bonding electrons, which results in slightly shorter Sb-C bond lengths (2.135(5), 2.146(5), 2.157(5), 2.165(5) Å) and wider C-Sb-Sb (89.1(1)°, 89.3(1)°) and C-Sb-C bond angles (100.3(2)°) for the fourfold-coordinated Sb center in **6** compared to the threefold-coordinated Sb atom (C-Sb-Sb 84.3(1)°, 84.7(1)°; C-Sb-C 92.9(2)°) and distibane **2** (Sb-C 2.1595(18) - 2.1695(18) Å; C-Sb-Sb 86.07(5) - 86.33(5)°, C-Sb-C 94.24(7), 95.39(7)°).[57]

Analogous trends were reported for $[Ph_4Sb_2][Fe(CO)_3PPh_3]$ (Sb-Sb 2.8282(7) Å vs. 2.844(1) Å for Sb_2Ph_4[95]), which showed comparable Sb-C bond lengths and C-Sb-C as well as C-Sb-Sb bond angles for the threefold- (Sb-C 2.138(9), 2.145(7) Å, C-Sb-Sb 94.9(2)°, 98.1(2)°, C-Sb-C 98.4(3)°) and fourfold-coordinated Sb atoms (Sb-C 2.130(6) Å, 2.132(7) Å, C-Sb-Sb 98.6(2)°, 100.0(2)°, C-Sb-C 100.5(2)°), respectively.[96] $[Me_4Sb_2][Cr(CO)_5]_2$[97] also showed shorter Sb-Sb and Sb-C bond lengths as well as wider C-Sb-C and C-Sb-Sb angles compared to Sb_2Me_4.[98] The Sb-Cr bond length in **6** (2.6084(9) Å) is comparable to those in $[R_4Sb_2][Cr(CO)_5]$ (R = Ph 2.625(3) Å;[99] R = Me 2.621(8), 2.629(9) Å),[100] and $[t\text{-}Bu(Cl)Sb]_2[Cr(CO)_5]$ (2.602(2) Å), respectively.[101] The Cr-CO_{trans} bond lengths in **4** (1.8663(18) Å, 1.858(2) Å) and $[Naph_2As_2]Cr(CO)_5$ in **5** (1.847(9) Å) are significantly shorter than the average Cr-CO_{trans} bond lengths in **4** (1.904 Å, 1.905 Å) and **5** (1.905 Å), whereas the differences observed for **6** (Cr-CO_{trans} 1.880(5) Å, av. Cr-CO_{trans} 1.902 Å) are smaller. This points to a stronger σ-donor/π-acceptor capacity of **1** compared to **2**, which agrees with results from IR spectroscopy.

6 shows intermolecular Sb···π interactions in the solid state and the Sb-$naph_{centr.}$ distance of 3.65 Å (centroid of C5 to C10) is comparable to those in $Naph_2Sb_2$ **2** (3.65/3.86 Å). Short CH···carbonyl interactions were observed (Figure 8), whereas no intermolecular As···π interactions were found in **4** and **5**.

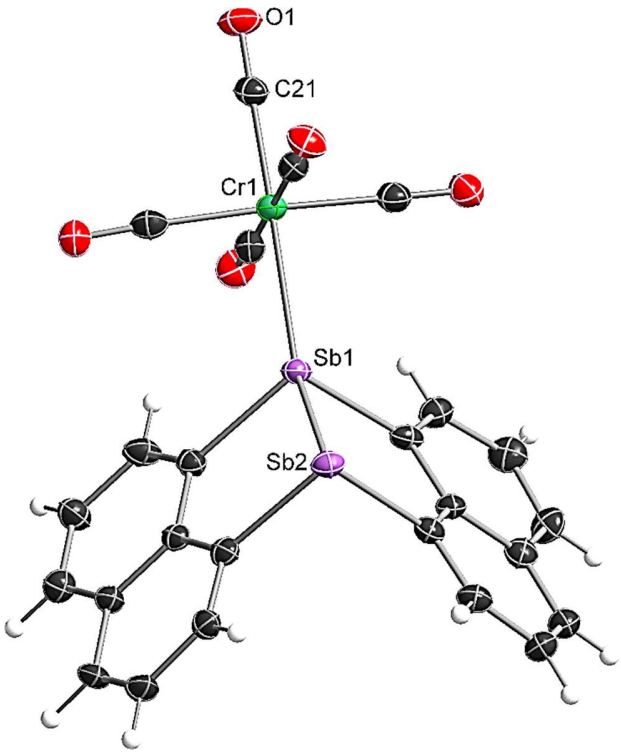

Figure 7. Molecular structure of 6 in the solid state. Co-crystallized solvent (CH_3CN) was omitted for clarity. Thermal ellipsoids are shown at the 50% probability level.

Table 2. Experimental [calculated][a] bond lengths [Å] and bond angles [°] of 4 - 8.

	4	5[c]	6	7	8
E-E[b]	2.4248(3) [2.443]	2.4324(11) [2.445]	2.7516(5) [2.772]	2.8383(4)[2.820]	4.948(9) [4.941]
E-C	1.9428(16) [1.953] 1.9366(15) [1.953] 1.9430(16) [1.959] 1.9548(16) [1.959]	1.942(8) [1.954] 1.947(8) [1.954] 1.954(8) [1.980] 1.965(8) [1.980]	2.146(5) [2.146] 2.135(5) [2.146] 2.157(5) [2.181] 2.165(5) [2.181]	1.988(3) [1.994] 1.987(3) [1.994] 1.981(3) [1.994] 1.983(3) [1.994]	2.171(3) [2.192] 2.179(2) [2.205]
E-Cr	2.4402(3) [2.421] 2.4687(4) [2.443]	2.4726(15) [2.436]	2.6084(9) [2.594]	-	-
E-Cl	-	-	-	2.2058(8) [2.244] 2.2016(8) [2.244]	2.3826(7) [2.411] 2.4604(7) [2.488] 2.3789(7) [2.414] 2.3872(7) [2.402]
C-E-E	90.89(5) [91.2] 91.55(5) [91.2] 90.89(5) [90.6] 90.41(5) [90.6]	91.8(2) [92.9] 92.7(2) [92.9] 89.1(2) [88.5] 88.9(3) [88.5]	89.3(1) [89.3] 89.1(1) [89.3] 84.7(1) [84.1] 84.3(1) [84.1]	-	-
C-E-C	100.54(8) [101.3] 101.21(7) [101.3]	103.2(3) [100.9] 95.7(3) [96.7]	100.3(2) [98.8] 92.9(2) [94.2]	96.0(1) [94.3] 95.9(1) [94.2]	-
M-E-E	122.10(1) [120.9] 131.79(1) [131.9]	130.41(5) [126.3]	139.34(2) [136.0]	-	-
M-E-C	123.35(5) [122.2] 120.64(6) [122.2] 117.21(6) [117.6] 118.28(6) [117.8]	116.6(2) [118.8] 116.4(2) [118.8]	115.7(1) [117.5] 115.0(1) [117.4]	99.7(1) [100.3] 99.7(1) [100.3] 99.9(1) [100.3] 99.27(9) [100.3]	93.63(7) [92.8] 94.07(7) [95.6] 96.12(6) [93.2] 94.43(7) [92.7]

[a] Calculated at the BP86-D3/def2-TZVPP level of theory (def2-QZVP for E = As, Sb). [b] E = As (**4**, **5**), Sb (**6**). [c] Only values of the mononuclear complex are given.

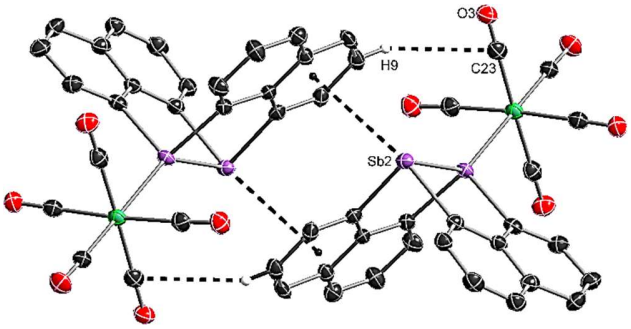

Figure 8. CH-carbonyl and Sb···π interactions in 6. All other hydrogen atoms were omitted for clarity. Thermal ellipsoids are shown at the 50% probability level.

Cangelosi *et al.* analyzed E···π interactions (As, Sb, and Bi) in a Cambridge Structural Database search. They are partially covalent in nature but primarily a dispersion interaction. The interaction distance is shorter for the heavier pnictogens due to the increasingly diffuse nature of the electron lone pair.[66] The structural findings of **4** to **6** point to a high p-orbital character of the bonding electrons in **4**, **5**, and **6** compared to **1** and **2**.

Calculated structures are denoted with an apostrophe, e.g. **X'**. Electron localization function (ELF) plots (Figure 9) in the Sb-Sb-Cr (a) and the C1-Sb-C1' planes (b) of **6'** as-defined in Figure S26 show a shift of the electron density on the Sb centers towards Cr, compared to **2'** (c, d). Higher electron pair density (shown in red) is found in bonds or electron lone-pairs.

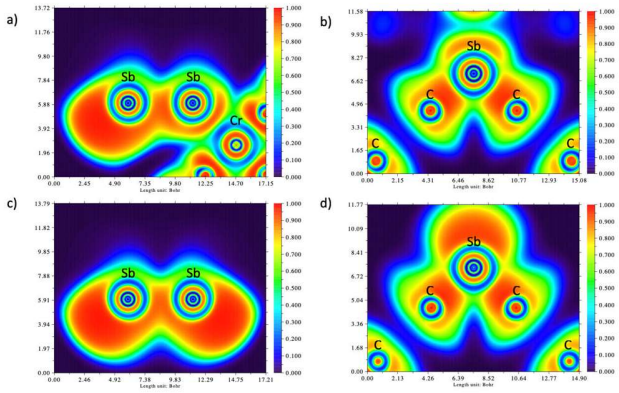

Figure 9. Electron localization function (ELF) plots in 6' (a) and b)) and 2' (c) and d)). Left: the bisecting molecular plane and in the C1-Sb1-C1' plane (right).

The ELF plots show the presence of lone pairs on the Sb atoms in **2'** and **6'**, as well as electron pair density between Sb and Cr in **6'**.

To study the electronic structures of **4** and **6** and the nature of the E-Cr bond in more detail, gas phase structures, natural population analysis (NPA) charges, and Wiberg bond indices (WBIs) of mononuclear $[Naph_2E_2]Cr(CO)_5$ (E = P, As **4'**, Sb, Bi) and binuclear complexes $[Naph_2E_2][Cr(CO)_5]_2$ (E = P, As, Sb **6'**, Bi) were calculated using density functional theory (DFT) at the BP86 def2-TZVPP (def2-QZVP for E) level of theory. Computed E-E bond lengths in **4'** and **6'** (Table 2) are roughly 0.02 Å (0.75%) longer and E-Cr bond lengths 0.02 Å (1%) shorter than those observed in the solid state, while the C-E-C, M-E-E and M-E-C bond angles deviate by less than 2°. Donor orbitals can be assigned to the pnictogen atoms. The P atom shows a lone pair participation on the HOMO, whereas the heavier congeners have lone pair participations on the HOMO-1 (Figure S28). With respect to the orbital energies, this agrees with the reduced σ-donor character of the heavier pnictogens. Natural bond orbital (NBO) analyses of mono- and binuclear complexes show that the lone pair of the pnictogen donates into the antibonding C-O_{trans}* acceptor orbital (Figure 10).

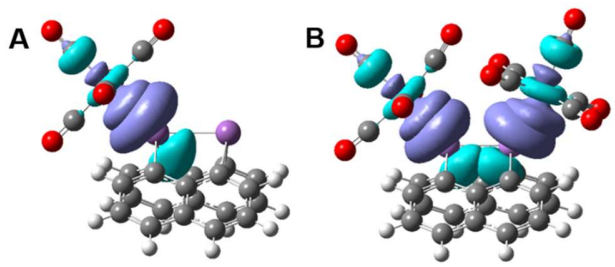

Figure 10. NBO interactions of lone pair (Sb1) into σ* Cr1-CO_{trans} (A) in 6 as well as both lone pairs (As1 and As2) into σ* Cr1-CO_{trans} (B) in 4 at an isovalue of 0.05.

The complexation reaction leads to a large increase of the NPA charges of the coordinating pnictogen atoms and a slight increase of the uncomplexed pnictogen atoms in the mononuclear complexes (Table 3).

Table 3. Differences in NPA charges of related atoms in mononuclear and binuclear chromium complexes compared to unsubstituted complexes $Naph_2E_2$.

Δq_{NPA}	P	As	Sb	Bi
E1[a]	+0.38	+0.35	+0.35	+0.26
E2[a]	+0.05	+0.05	+0.08	+0.11
Cr[a]	−0.65	−0.63	−0.62	−0.56
E1[b]	+0.40	+0.44	+0.40	+0.34
E2[b]	+0.37	+0.41	+0.38	+0.31
Cr1[b]	−0.65	−0.64	−0.62	−0.55
Cr2[b]	−0.62	−0.62	−0.63	−0.56
BDE[a]	199	174	161	131
BDE[b]	186	168	149	109

[a] $Naph_2E_2Cr(CO)_5$; [b] $Naph_2E_2[Cr(CO)_5]_2$, BDE = E-Cr bond dissociation energy (kJ/mol). E1 denotes to the substituted pnictogen atom in mononuclear compound.

Note that positive values indicate a decrease in the charge density and therefore less electrostatic repulsion of the two pnictogen centers, which corresponds to the slightly shorter Sb-Sb bond in **6** compared to **2**. The increase of the NPA charge reflects the electron donating character of the pnictogen atoms to the chromium center. However, a linear trend was not observed from phosphorous to bismuth. Coordination of $Cr(CO)_5$ results in a decrease of the energy of the HOMO and HOMO-1 for the mononuclear complexes (Figure S29). Calculated WBIs of mononuclear $Naph_2E_2[Cr(CO)_5]$ and binuclear complexes $Naph_2E_2[Cr(CO)_5]_2$ show a slight decrease of the E-E bond order compared to $Naph_2E_2$ (Table S5). The E-Cr bond dissociation energies within $Naph_2E_2[Cr(CO)_5]$ were calculated as stated in the electronic supplement and steadily decrease from phosphorous to bismuth (E-Cr = 199 (P), 174 (As), 161 (Sb) and 131 (Bi)) in accordance with the decreasing donor character. The calculations agree with our experimental findings with respect to the σ-donor/π-acceptor character in **4** and **6**. Note that the second bond dissociation energy is smaller in all cases, proving the reduced σ-donor ability of the dipnictane after the first complexation. The results also indicate that binuclear complexes should be generally less accessible. The E-Cr dissociation energies within $Naph_2E_2[Cr(CO)_5]_2$ steadily decrease from P to Bi (E-Cr = 186 (P), 168 (As), 149 (Sb) and 109 (Bi)). However, in spite of the fairly large positive BDEs for all computed structures, there is no evidence for the existence of binuclear Sb and Bi complexes, indicating that the stability predicted by simple electronic structure calculations might actually be significantly smaller, either due to errors in the DFT energies or by other effects like solvation.

Oxidation reactions of $Naph_2E_2$ – Enhanced dispersion in the intermolecular interactions and its origin

We became further interested to compare the reactivity of **1** and **2** with that of $Naph_2P_2$. $Naph_2P_2$ was found to react with AuCl(tht) (tht = tetrahydrothiophene) with formation of the binuclear complex $Naph_2P_2(AuCl)_2$[59] as was observed in the reaction of $Naph(PPh)_2$, which gave $Naph(PPh)_2(AuCl)_2$.[102] In contrast, the reaction of **1** with Me_2SAuCl proceeded with reduction of Me_2SAuCl, oxidative cleavage of the As-As bond and formation of $Naph_2(AsCl)_2$ **7** (Scheme 5).

Scheme 5. Synthesis of 7 by oxidation reaction of 1 with Me_2SAuCl.

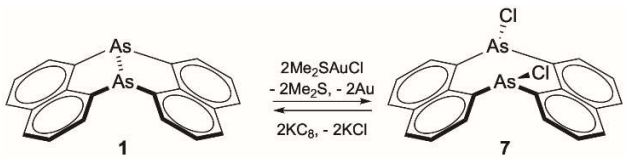

7 is soluble in CH_2Cl_2 and $CHCl_3$ and was obtained as yellow crystalline solid after workup in excellent yield (85%). The ^1H and ^{13}C resonances of the Naph substituents of **7** are shifted to lower field compared to those of **1** (Table S1, S2). **7** shows two doublets (8.13, 7.82 ppm) and one triplet (7.56 ppm). Reduction of **7** by reaction with an excess of KC_8 in benzene solution again gave **1** in almost quantitative yield.

Crystals of **7** (Figure 11) were grown from a solution in $CHCl_3$ upon storage at 0 °C for 24 h. **7** crystallizes in the triclinic space group *P*-1 with two molecules in the unit cell.

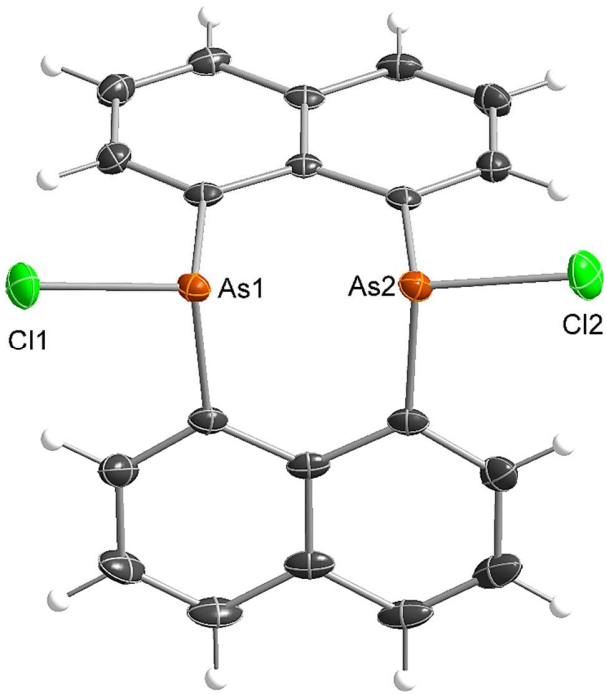

Figure 11. Molecular structure of 7 in the solid-state. Thermal ellipsoids are shown at the 50% probability level.

The As-As distance in **7** (2.8383(4) Å) is elongated by 40 pm compared to that in **1** (2.4326(4) Å). A more pronounced bond length elongation is hampered by the rigid Naph ligands, which fix the As atoms to a distinct distance. The As-C (1.981(3) – 1.988(3) Å) and As-Cl bond lengths (2.2058(8), 2.2016(8) Å) are within the expected range. The sum of the bond angles at both As centers in **7** (295.4(3)°, 295.07(12)°) is larger compared to those in **1** (267.88(17)° and 266.57(17)°). In remarkable contrast to **1**, intermolecular As···π interactions (As-naph$_{centr.}$ distance 3.628(8) and 3.578(9) Å) were observed in **7** (Figure 12), which is comparable to As···π interactions previously reported.[103,104]

The electronic structure of **7'** was therefore calculated as a dimer as shown in Figure 12 at the BP86 def2-TZVPP (def2-QZVP for E) level of theory and selected bond lengths and angles are summarized in Table 2. Compound **7'** shows a small deviation in the computed E-E distances (0.02 Å) compared to **7**. The deviation of the M-E-E and M-E-C bond angles is 1°, while C-E-C angles deviate by 2.2°.

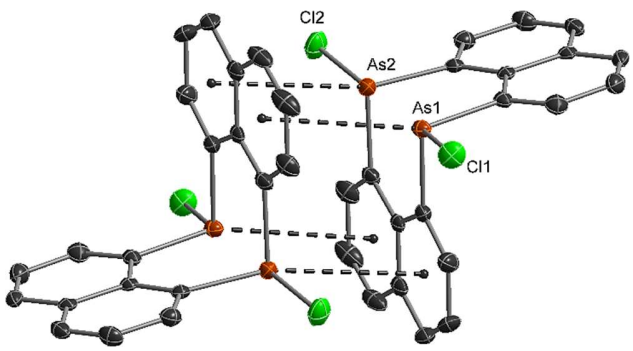

Figure 12. As···π interactions in the solid state of 7. Hydrogen atoms were omitted for clarity. Thermal ellipsoids are shown at the 50% probability level.

In Figure 13 the electron localization function along two planes (definition Figure S27) in **7'** (a,b) and **1'** (c,d) are compared. ELF plots show reduced electron density on the As-As axis between the As atoms upon oxidation of the As atoms and formation of two terminal As-Cl bonds. The structure of the lone pair density reflects the properties of a σ-hole being formed adjacent from an electronegative binding partner at the pnictogen atom, which should also increase its ability to act as an electron acceptor, in line with increasing NPA charges from 0.49 (**1'**) to 0.89 (**7'**) for the As atoms.

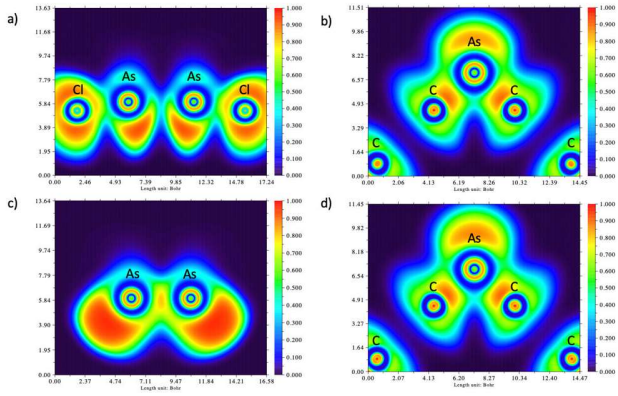

Figure 13. Electron localization function (ELF) plots in 7' (a) and b)) and 1' (c) and d)). Left: the bisecting molecular plane and in the C1-As-C1' plane (right).

A comparison of the DLPNO-CCSD(T) LED of the intermolecular interaction in dimers of **7'** and **1'** (Figure 14) shows a remarkable change in the intermolecular interaction. While there is a slight increase in repulsive (HF interaction from 57 kJ/mol to 65 kJ/mol) and attractive non-dispersive contributions (from –11 kJ/mol to –16 kJ/mol), the dispersion contribution increases from –97 kJ/mol to –120 kJ/mol and, as a consequence, also the total interaction energies increase from –69 kJ/mol to –92 kJ/mol.

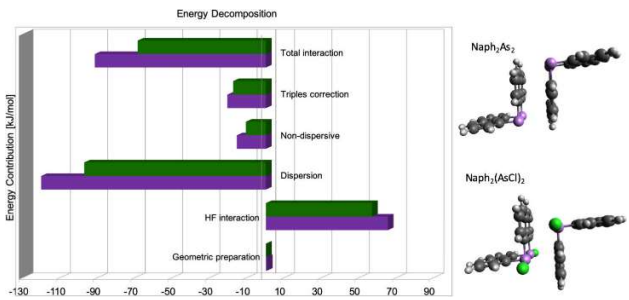

Figure 14. DLPNO-CCSD(T) LED-analysis of the Naph$_2$As$_2$ dimer 1' (green) and Naph$_2$(AsCl)$_2$ 7' (purple) (geometries optimized at the level BP86 def2/TZVPP of theory, DLPNO-CCSD(T)/cc-pVTZ using tight PNO settings).

Figure 15 shows the dispersion interaction density (DID)[105,80] for both compounds, which displays the sum of the pair contributions to dispersion as a map on the localized orbitals. This suggests an overall increase of delocalized contributions and clearly shows the additional contribution of the chlorine atoms to the dispersion interaction. The overall increase of dispersion upon oxidation of the As atoms is quite remarkable since the charge density at the As atoms is reduced with dispersion being related to the polarizability of the atom.

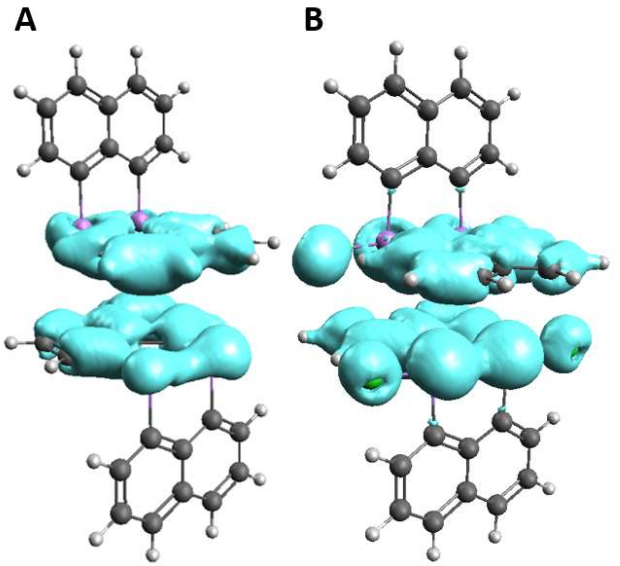

Figure 15. Dispersion interaction density (DID) computed at the DLPNO-CCSD/cc-pVTZ level of theory (normal PNO settings, strong pair contributions) of the $Naph_2As_2$ dimer 1' (A) and $Naph_2(AsCl)_2$ 7' (B); geometries optimized at the level BP86 def2/TZVPP of theory.

In order to understand this effect in more detail, a DLPNO-CCSD(T) LED fragment analysis has been carried out for four systems: The dimers **1'** and **7'** as well as two artificial dimer structures resulting from removing the chlorine atoms from **7'** and from adding chlorine atoms to dimer **1'** at the bond lengths and angles found in dimer **7'**. The results are displayed in Figure 16. This way, geometrical factors, the influence of the different fragments and electronic effects can be studied separately.

The analysis shows that abstraction of the chlorine and reduction of the arsenic atoms in the original structure of dimer **7'** (Figure 16 top left and top right) leaves the Naph-Naph dispersion interaction almost unchanged, whereas the As-Naph dispersion contribution is reduced by 10 kJ/mol as is expected. However, the overall interaction energy also is strongly reduced, as the contribution of the pair of Cl-Naph dispersion interactions, which sums up to –24 kJ/mol, overcompensates this. Comparing the structure on the top left of Figure 16 to dimer **1'** (bottom right) it becomes obvious that the equilibrium structure of dimer **1'** is a result of maximized dispersion interaction between the Naph moieties balancing the As···π interaction. Adding Cl atoms to this structure (see Figure 16 bottom left) results in slightly reduced Naph-Naph and As-Naph dispersion interactions, but the Cl···π interaction (–16 kJ/mol) increases the dispersive intermolecular interaction.

Hence, while oxidation of the As atoms decreases their contribution to the dispersion interaction as expected, the increased overall dispersion interaction originates from the additional Cl···π contribution present in dimer **7'**. In dimer **1'**, which lacks this component, the balance between As···π and π···π interactions leads to a different intermolecular arrangement with an offset geometry and decreased overall interaction energy.

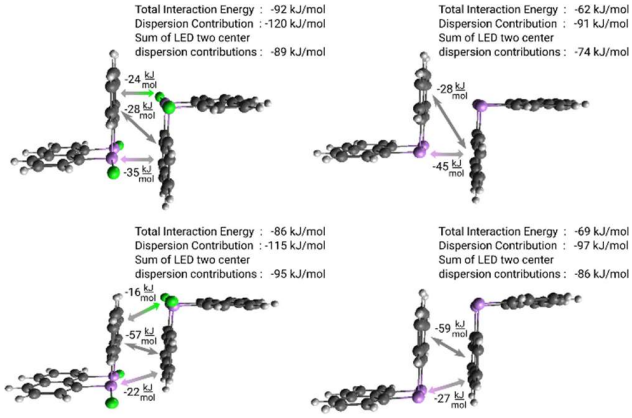

Figure 16. DLPNO-CCSD(T) fragment LED for four dimer structures: top left – dimer 7', bottom right – dimer 1', bottom left –dimer 1' with two Cl atoms added at the corresponding bond distances and angles, top left - dimer 7' with two Cl atoms removed. The As atoms, the Cl atoms and the Naph moieties have been chosen as fragments. Grey-green arrows denote the sum of all Cl-Naph dispersion-type two-fragment interactions, grey arrows denote the corresponding Naph-Naph and pink-grey the corresponding As-Naph interaction contributions. Note that the sum of the two-center contributions is smaller than the total dispersion interaction between the monomers due to contributions that originate from amplitudes for which the orbitals are located on more than two fragments.

In contrast to the reaction of $Naph_2As_2$ **1**, the reaction of $Naph_2Sb_2$ **2** with Me_2SAuCl yielded a complex reaction mixture, from which no defined product could be isolated (Figure S24), to date. Therefore, the influence of two Cl substituents in the hypothetic Sb(III) molecule $Naph_2(SbCl)_2$ on the dispersion interaction could not be investigated. In contrast, the reaction of $Naph_5Sb_4Cl_2$ **3** with Me_2SAuCl occurred with clean formation of elemental gold, perylene and $[NaphSbCl_2]_2$ **8** (Scheme 6). As was observed in the reaction with $Naph_2As_2$ **1**, Me_2SAuCl served as weakly oxidizing agent, resulting in a C-C coupling reaction. Resonances of the Naph substituents in the ^1H and ^{13}C NMR spectra of **8** are shifted to lower field compared to those of **3** (Table S1, S2) as was observed for **7**. **8** shows three doublets (8.81, 8.21, 8.10 ppm) and a series of signals between 7.86 and 7.67 ppm.

Scheme 6. Synthesis of 8 by oxidation reaction of 3 with Me_2SAuCl.

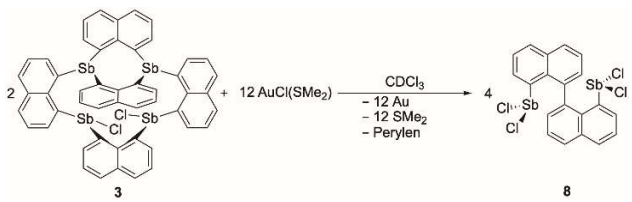

Single crystals of **8** (Figure 17) were grown from a solution in $CHCl_3$ upon storage at 0 °C for 24 h. **8** crystallizes in the triclinic space group *P*-1 with two molecules in the unit cell. The 1,1'-binaphthyl ligand in **8** is coordinated by two $SbCl_2$ units in position 8 and 8' and the aromatic systems show a torsion angle of 105.8°. The Sb-C bond lengths (2.171(3), 2.179(2) Å) are comparable to those of **2** (2.160(2) - 2.169(2) Å) and **3** (2.134(8)

- 2.206(9) Å). **8** adopts a dimeric structure with a centrosymmetric Sb_2Cl_2 four-membered ring, and the terminal Sb-Cl bonds (2.3826(7), 2.3789(7), 2.3872(7) Å) are shorter than the bridging Sb-Cl bond (2.4604(7) Å).

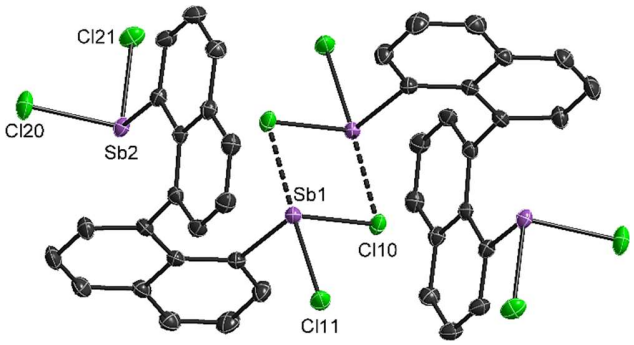

Figure 17. Molecular structure of compound 8 in the solid-state. Hydrogen atoms were omitted for clarity. Thermal ellipsoids are shown at the 50% probability level.

The electronic structure of **8'** was also calculated as a dimer as shown in Figure 17 at the BP86 def2-TZVPP (def2-QZVP for E) level of theory and selected bond lengths and angles of the computed structure, which deviate by approximately 1% from those in the solid state, are summarized in table 2. Both the solid-state and the calculated structures show one bridging Sb-Cl bond, which is elongated by about 7 pm compared to the terminal Sb-Cl bonds (2.4604(7) Å). The Sb···π contacts observed in the solid state structure of **8** (3.048(7) Å) and in the computed structure **8'** (3.090 Å) are significantly shorter compared to those observed in **2** (3.65/3.86 Å) and **6** (3.65 Å) as well as to those previously reported,[106-109] respectively.

In order to study the nature of the Sb···π interaction in **8** in more detail, we choose to model the intramolecular interaction using a system which allows to assess the different components as separate, intermolecular contributions (see Figure 18). This allows an easier quantification of the different interactions in terms of strain in the subsystem, charge-transfer between the fragments and dispersion interaction. **8'** was decomposed into three fragments, which were optimized in the starting geometry of **8'** in order to ensure not to be too far from a physically meaningful structure, and the total interaction energy was used as well as the D3 dispersion correction as an estimate for the intermolecular interactions in **8'**.

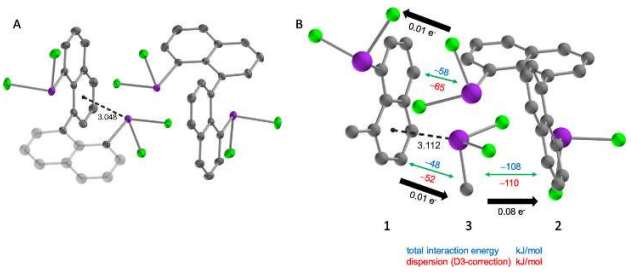

Figure 18. XRD-structure of 8 (A) and fragments of model system 8' (B) in optimized geometry with related total interaction energies and dispersion correction in kJ/mol as well as electron transfer between each pair of fragments.

The results show the strong structure determining role of dispersion interaction. Almost no electron transfer regarding the Sb atoms is denoted, since the NPA charges on all Sb atoms increase by only 0.01 units in fragment combinations of **8'**, compared to the single fragments without interactions. Furthermore, intermolecular Sb···Cl contacts largely contribute to the dimerization of **8** in the solid-state and the rigid molecular framework provokes a strained geometry in the dimer of **8**, which enhance intra- and intermolecular contacts and therefore favor dispersion related Sb···π interactions. These play a significant structural relating role in the dimer of **8**, compared to less dominant charge-transfer induced effects, which are in the range of 0.01 to 0.08 electrons depending on the chosen model system. This is in good agreement with comparable values for intermolecular interactions of antimony with π-arenes, for which comparable Sb···π interactions have been characterized as predominantly dispersive with interaction energies in the order of 20-30 kJ/mol per contact.[66]

CONCLUSION

Our general interest in the nature of metal···π interactions has stimulated this research on the synthesis and reactivity of naphthalene-based group 15 complexes $Naph_2E_2$. $Naph_2As_2$ **1** was synthesized by reaction of $NaphLi_2(TMEDA)$ with $AsCl_3$ and the observed intermolecular CH···π and π···π interactions in the solid state as well as the missing As···π interactions perfectly agree with the previously predicted structure.[55] The σ-donor properties of $Naph_2As_2$ **1** and $Naph_2Sb_2$ **2** were studied in reactions with $coeCr(CO)_5$, yielding binuclear $Naph_2As_2[Cr(CO)_5]_2$ **4** and mononuclear complexes $Naph_2E_2Cr(CO)_5$ (E = As **5**, Sb **6**). In agreement with the nature and relative energies of the donor orbitals, the sigma-donor character decreases down the periodic table from As to Sb to Bi. In remarkable contrast, the reaction of **1** with Me_2SAuCl occurred with oxidation of the As atoms and formation of $Naph_2(AsCl)_2$ **7**, which shows distinct As···π interactions in the solid-state, whereas **3** was found to react with Me_2SAuCl with C-C coupling and formation of elemental gold, perylene and $[NaphSbCl_2]_2$ **8**, respectively.

The electronic structure of **1'** to **8'** was analyzed by detailed quantum chemical calculations, including NBO and ELF analyses at the BP86-D3/def2-TZVPP level of theory and Local Energy Decomposition at the DLPNO-CCSD(T)/cc-pVTZ level of theory. Remarkably, the change in electronic structure upon oxidation of the As centers from As(II) to As(III) in $Naph_2(AsCl)_2$ **7'** goes along with a significant increase of the dispersion contributions, which increase by 25% compared to the dispersion interaction in $Naph_2As_2$. In contrast, $Naph_2As_2$ **1** does not exhibit any As···π interactions in the crystal structure. A DLPNO-CCSD(T) fragment LED on a series of structures reveals that this remarkable increase of the dispersion interaction in **7** occurs mostly due to the contribution of the additional chlorine atoms, while the As···π contribution actually decreases, as expected. In contrast to this, the equilibrium structure of **1** is determined by the balance of As···π and π··π interactions, for which the latter are roughly a factor of two larger, hence no As···π interactions are observed in the crystal structure.

EXPERIMENTAL SECTION

All manipulations were performed in a Glovebox (MBraun) under an Ar atmosphere and with standard Schlenk techniques. Solvents were carefully dried over Na/K alloy and degassed prior to use. Chloroform was dried over CaH_2 and stored over molar sieve. Acetonitrile was dried and stored over molar sieve. $Naph_2Sb_2$ **2**[57] and $coeCr(CO)_5$ (coe = *Z*-cyclooctene)[110] were prepared according to literature methods, whereas Me_2SAuCl was commercially available (abcr) and used as received. NMR spectra were recorded on a Bruker Avance 300 spectrometer at 25 °C at 300.1 MHz (^1H) and

75.5 MHz (^{13}C) and are referenced to internal $CDCl_3$ (^1H, δ = 7.254; ^{13}C, δ = 77.230). IR spectra were recorded on a Bruker ALPHA-T FT-IR spectrometer equipped with a single reflection ATR sampling module.

Synthesis of $Naph_2As_2$ 1. A solution of $AsCl_3$ (2 mmol, 363 mg) in 10 ml of THF was added dropwise to a cooled solution (−78 °C) of $Li_2Naph(TMEDA)$ (3 mmol, 769 mg) in 10 ml of THF and then warmed to ambient temperature within 12 h. After additional stirring at room temperature for 6 h, all volatiles were removed *in vacuo* and the resulting orange solid was repeatedly washed with hexane (3 x 20 ml). After extraction with 30 ml of fluorobenzene, the orange residue was re-crystallized from a solution in $CHCl_3$ at 0 °C, yielding light-orange crystals after 12 h. Yield: 258 mg (0.52 mmol, 52%). M.p. = 189 °C. Anal. Calcd. for $C_{20}H_{12}As_2$: C, 59.73; H, 3.01; Found: C: 59.81; H: 3.00; ^1H NMR ($CDCl_3$, 25 °C, 300 MHz): δ 7.99 (d, $^3J_{HH}$ = 7.0 Hz, 4 H, 4,5-Naph-H), 7.63 (d, $^3J_{HH}$ = 8.3 Hz, 4 H, 2,7-Naph-H), 7.40 (t, $^3J_{HH}$ = 8.2 Hz, 4 H, 3,6-Naph-H). ^{13}C NMR ($CDCl_3$, 75 MHz, 25 °C): δ 149.9 (10-Naph-C), 141.4 (9-Naph-C), 135.5 (2,7-Naph-C), 131.3 (1,8-Naph-C), 127.9 (4,5-Naph-C), 126.9 (3,6-Naph-C). FT-IR: ν 3053, 2962, 1259, 1086, 1015, 796, 766, 703 cm^{-1}.

Synthesis of $Naph_5Sb_4Cl_2$ 3. A solution of $SbCl_3$ (0.8 mmol, 183 mg) in 10 ml of Et_2O was added dropwise to a cooled solution (−78 °C) of Li_2Naph (1 mmol, 140 mg) in 10 ml Et_2O and warmed to ambient temperature within 12 h. After additional stirring for 6 h, all volatiles were removed *in vacuo* and the resulting residue was washed with hexane (3 x 20 ml). After extraction with hot chloroform (20 ml), the yellow residue was crystallized from a solution in $CHCl_3$ at 0 °C. Yield 164 mg (138 mmol, 69%). M.p. = >250 °C. Anal. Calcd. for $C_{50}Sb_4Cl_2H_{30}$: C: 50.52; H: 2.54; Found: C: 50.43; H: 2.32; ^1H NMR ($CDCl_3$ / Tol-d_8 1:5, 70 °C, 300 MHz): δ 8.57 (dd, $^3J_{HH}$ = 7.1, 1.3 Hz, 4 H, 2,7-Naph-H), 8.08 (dd, $^3J_{HH}$ = 6.9, 1.1 Hz, 4 H, 4,5-Naph-H), 7.59 (dd, $^3J_{HH}$ = 8.2, 1.2 Hz, 6 H, 3,6-Naph-H), 7.47 (dd, $^3J_{HH}$ = 6.6, 2.7 Hz, 6 H, 2,7Naph-H), 7.41-7.34 (m, 10 H, 3,6-Naph-H). A ^{13}C NMR spectrum could not be recorded due to the low solubility of **3**. FT-IR: ν 3043, 2327, 2233, 2219, 2084, 2065, 2026, 1992, 1716, 1587, 1536, 1482, 1435, 1345, 1329, 1310, 1242, 1194, 1139, 1042, 979, 922, 808, 761, 672, 614, 540, 516, 460, 430, 401 cm^{-1}.

Synthesis of $Naph_2As_2[Cr(CO_5)]_2$ 4. A solution of $coeCr(CO)_5$ (0.1 mmol, 30 mg) in 5 ml of CH_2Cl_2 was added to a solution of $Naph_2As_2$ (**2**) (0.05 mmol, 20 mg) in 5 ml of CH_2Cl_2 and stirred for 12 h. All volatiles were removed *in vacuo* and the resulting yellow solid was dissolved in 10 mL of $CHCl_3$. Single crystals were obtained after concentration to 5 mL and storage at 0 °C for 12h. Yield: 26 mg (0.033 mmol, 66%). M.p. = 208 °C (dec.). Anal. Calcd. for $C_{30}H_{12}Cr_2O_{10}As_2$: 45.83; H, 1.54. Found: C. 46.01; H: 1.62%. ^1H NMR (CD_2Cl_2, 25 °C, 300 MHz): δ 8.15 (d, $^3J_{HH}$ = 6.9 Hz, 4 H, 4,5-Naph-H), 7.82 (d, $^3J_{HH}$ = 7.90 Hz, 4 H, 2,7-Naph-H), 7.59 (t, $^3J_{HH}$ = 8.1 Hz, 4 H, 3,6-Naph-H). ^{13}C NMR (CD_2Cl_2, 75 MHz, 25 °C): δ 221.1 (CO), 215.7 (CO) 144.1 (10-Naph-C), 136.6 (9-Naph-C), 134.7 (2,7-Naph-C), 131.5 (1,8-Naph-C), 130.4 (4,5-Naph-C), 126.7 (3,6-Naph-C). FT-IR (solid-state): ν 3053, 2923, 2064, 1992, 1910, 1587, 1486, 1444, 1365, 1325, 1260, 1206, 1147, 1081, 1016, 906, 862, 816, 764, 666, 645, 545, 448 cm^{-1}. FT-IR ($CDCl_3$ solution): 2064, 1949, 1262, 815, 740, 667, 460, 442 cm^{-1}.

Synthesis of co-crystallized $Naph_2As_2[Cr(CO_5)]_2$ 4 and $Naph_2As_2[Cr(CO_5)]$ 5. A solution of $coeCr(CO)_5$ (0.09 mmol, 27 mg) in 5 ml of CH_2Cl_2 was added to a solution of $Naph_2As_2$ (**2**) (0.1 mmol, 21 mg) in 5 ml of CH_2Cl_2 and stirred for 12 h. All volatiles were removed *in vacuo* and the resulting yellow solid was dissolved in 10 mL of $CHCl_3$. Single crystals were obtained after concentration to 5 mL and storage at 0 °C for 12 h. Yield: 41 mg (0.030 mmol, 33%). M.p. = 210 °C (dec.). Anal. Calcd. for $C_{55}H_{24}As_4Cr_3O_{15}$:C, 47.85; H, 1.75%. Found: C. 48.12; H: 1.82%. ^1H NMR ($CDCl_3$, 25 °C, 300 MHz): δ 8.17 (d, $^3J_{HH}$ = 7.2 Hz, 4 H, 4,5-Naph-H (**4**)), 7.85 (d, $^3J_{HH}$ = 7.6 Hz, 4 H, 2,7-Naph-H (**4**)), 7.55 (t, $^3J_{HH}$ = 8.0 Hz, 4 H, 3,6-Naph-H (**4**)), δ 8.11 (dd, $^3J_{HH}$ = 7.0, 0.8 Hz, 2 H 4-Naph-H (**5**)), 8.05 (dd, $^3J_{HH}$ = 6.9, 0.8 Hz, 2 H, 5-Naph-H (**5**)), 7.75 (dd, $^3J_{HH}$ = 12.5, 7.6 Hz, 2 H, 3-Naph-H (**5**)), 7.64 (d, $^3J_{HH}$ = 7.2 Hz, 4 H, 2,7-Naph-H (**5**)), 7.49 (dd, $^3J_{HH}$ = 8.1, 7.0 Hz, 2 H, 6-Naph-H (**5**)). ^{13}C NMR ($CDCl_3$, 75 MHz, 25 °C): δ 144.5 (10-Naph-C (**4**)), 139.2 (9-Naph-C (**4**)), 135.1 (2,7-Naph-C (**4**)), 132.0 (1,8-Naph-C (**4**)), 130.8 (4,5-Naph-C (**4**)), 128.1 (3,6-Naph-C (**4**)), 147.1 (10-Naph-C (**5**), 146.7 (9-Naph-C (**5**)), 137.0 (1-Naph-C (**5**)), 135.5 (8-Naph-C (**5**)), 132.2 (4-Naph-C (**5**)), 131.4 (2,7-Naph-C (**5**)), 130.2 (6-Naph-C (**5**)), 129.1 (3-Naph-C (**5**), 127.8 (5-Naph-C (**5**)). FT-IR: ν 3051, 2961, 2922, 2851, 2071, 2061, 1985, 1907, 1584, 1548, 1483, 1444, 1366, 1347, 1325, 1259, 1203, 1085, 1015, 930, 914, 862, 809, 763, 669, 643, 580, 545, 456, 447 cm^{-1}.

Synthesis of $Naph_2Sb_2[Cr(CO)_5]$ 6. A suspension of $Naph_2Sb_2$ (**2**) (0.5 mmol, 248 mg) in 50 ml of CH_2Cl_2 was combined with a solution of $coeCr(CO)_5$ (1.0 mmol, 302 mg) in 20 ml of CH_2Cl_2 and stirred for 12 h. All volatiles were removed *in vacuo* and the resulting yellow solid was dissolved in CH_3CN. Single crystals were obtained after concentration and storage at 0 °C for 48 h. Yield: 240 mg (0.355 mmol, 71 %). M.p. = 231 °C (dec.). Anal. Calcd. for $C_{25}H_{12}CrO_5Sb_2$: C, 43.65; H, 1.76. Found: C: 43.81; H: 1.79%. ^1H NMR ($CDCl_3$, 25 °C, 300 MHz) δ 8.14 (dd, $^3J_{HH}$ = 6.9, 1.2 Hz, 2 H, 4-Naph-H), 8.10 (dt, $^3J_{HH}$ = 6.9, 1.2 Hz, 2 H, 5-Naph-H), 7.82 (dd, $^3J_{HH}$ = 8.3, 1.1 Hz, 2 H, 3-Naph-H), 7.74 – 7.38 (m, 6 H, 2,6,7-Naph-H). ^{13}C NMR ($CDCl_3$, 75 MHz, 25 °C): δ 217.4 (CO), 216.3 (CO), 138.0 (9-Naph-C), 137.0 (10-Naph-C), 136.6 (1-Naph-C), 131.7 (8-Naph-C), 131.3 (4-Naph-C), 130.5 (5-Naph-C), 129.7 (3-Naph-C), 127.4 (2-Naph-C), 127.0 (7-Naph-C), 126.8 (6-Naph-C). FT-IR (solid-state): ν 3054, 2962, 2070, 2057, 1999, 1991, 1942, 1925, 1889, 1587, 1484, 1440, 1349, 1320, 1259, 1144, 1013, 866, 807, 794, 767, 735, 666, 641, 535, 519, 461, 436 cm^{-1}. FT-IR ($CDCl_3$ solution): 2066, 1946, 1261, 1089, 1033, 1008, 955, 889, 809, 669, 615, 544 cm^{-1}.

Synthesis of $Naph_2As_2Cl_2$ 7. $Naph_2As_2$ (**1**) (0.05 mmol, 20 mg) was suspended in 0.5 ml of d_2-dichloromethane in a J-Young NMR tube. Me_2SAuCl (0.1 mmol, 30 mg) was added and the reaction mixture was mixed by vigorous shaking. After 1h the precipitation of elemental gold was observed, and the reaction was completed after 24 h. All volatiles were removed *in vacuo* and the resulting solid was extracted with $CHCl_3$. Single crystals (yellow) were obtained after storage at 0 °C for 24 h. Yield: 20 mg (0.042 mmol, 85 %). M.p. = 205 °C. Anal. Calcd. for $C_{20}H_{12}As_2Cl_2$: C, 50.78; H, 2.56. Found: C: 50.91; H: 2.61%. ^1H NMR (CD_2Cl_2, 25 °C, 300 MHz): δ 8.13 (d, $^3J_{HH}$ = 7.09 Hz, 4 H, 4,5- Naph-H), 7.82 (d, $^3J_{HH}$ = 8.25 Hz, 4 H, 2,7-Naph-H), 7.56 (t, $^3J_{HH}$ = 7.59 Hz, 4 H, 3,6-Naph-H). ^{13}C NMR (CD_2Cl_2, 75 MHz, 25 °C): δ 138.0 (10-Naph-C), 135.2 (9-Naph-C), 132.1 (2,7-Naph-C), 130.0 (1,8-Naph-C), 127.4 (4,5-Naph-C), 125.9 (3,6-Naph-C). FT-IR: ν 3054, 2961, 1482, 1420, 1360, 1259, 1088, 1015, 863, 795, 762, 705, 543, 515, 400 cm^{-1}.

Synthesis of $(NaphSbCl_2)_2$ 8. $Naph_5Sb_4Cl_2$ (**3**) (0.05 mmol, 25 mg) was loaded into a J-Young type NMR tube and suspended in 0.5 ml CD_2Cl_2. Me_2SAuCl (0.3 mmol, 88 mg) was dissolved in 0.1 ml CD_2Cl_2 and added to the suspension. The mixture was shaken vigorously to become homogeneous. After 1 h, the formation of elemental gold was observed, and the reaction was completed after 24 h. All volatiles were removed *in vacuo* and the resulting solid was extracted with $CHCl_3$. Single crystals (yellow) were obtained after storage at 0 °C for 1 h. Yield: 29 mg (0.0455 mmol, 91%). M.p. = 257 °C. Anal. Calcd. for $C_{20}H_{12}Sb_2Cl_4$: C, 37.67%; H, 1.90. Found: C: 38.01%; H: 1.95%. ^1H NMR ($CDCl_3$, 25 °C, 300 MHz) δ 8.81 (dd, $^3J_{HH}$ = 7.2, 1.3 Hz, 2 H, 2-Naph-H), 8.21 (dd, $^3J_{HH}$ = 8.1, 1.5 Hz, 2 H, 5-Naph-H), 8.10 (dd, $^3J_{HH}$ = 8.2, 1.1 Hz, 2 H, 4-Naph-H), 7.86 – 7.67 (m, 6 H, 3,6,7-Naph-H). ^{13}C NMR ($CDCl_3$, 75 MHz, 25 °C): δ 152.3 (8-Naph-C), 137.6 (3,6-Naph-C), 137.0 (1,8-Naph-C), 136.6 (4,5-Naph-C), 136.5 (9,10-Naph-C), 133.4 (2,7-Naph-C), 131.8 (2,7-Naph-C), 131.7, (1,8-Naph-C), 128.8 (4,5-Naph-C), 127.8 (3,6-Naph-C). FT-IR: ν 3054, 2962, 1587, 1539, 1488, 1418, 1338, 1260, 1198, 1087, 1017, 923, 866, 808, 768, 655, 644, 626, 584, 532, 514, 477, 449 cm^{-1}.

Single Crystal X-ray Diffraction. The crystals were mounted on nylon loops in inert oil. Data were collected on an AXS D8 Kappa diffractometer with an APEX2 detector (MoKα radiation, λ =

0.71073 Å; T = 100(1) K). The structures were solved by Direct Methods (SHELXS-97) and refined by full-matrix least-squares on F^2.[111-113] Absorption corrections were performed semiempirically from equivalent reflections on the basis of multiscans (Bruker AXS APEX2). All non-hydrogen atoms were refined anisotropically, hydrogen atoms by a riding model (SHELXL-97/SHELXL-2013). In **3** the diffraction pattern showed signs of non-merohedral twinning however attempts to separate two independent lattices failed. Quantitative results should be critically accessed. The crystal of **6** was a non-merohedral twin of four components. The model was refined against HKLF5 data. In **8** the high residual density in close proximity to Sb1 is likely related to Fourier truncation effects. Different ways of absorption correction had no effect on the peak. On the crystal of **5** grew a fairly large satellite that could not be removed. The reflections of this satellite were too weak to successfully being treated as a twin component. However, they were strong enough to produce several poorly matching reflection due to overlap. Thus quantitative results should be carefully interpreted and might be unreliable.

CCDC-1907994 (**1**), -1907995 (**3**), -1907996 (**4**), -1907997 (**6**), -1907998 (**7**), -1907999 (**8**) and -1908000 (**5**) contain the supplementary crystallographic data for this paper. These data can be obtained free of charge from The Cambridge Crystallographic Data Centre via www.ccdc.cam.ac.uk/data_request/cif.

Quantum chemical calculations. Quantum chemical calculations were employed with ORCA quantum chemistry package (version 4.0).[114] The ground-state geometry optimizations were based on the solid-state structures obtained by single-crystal x-ray diffraction. All structural optimizations were performed in with the BP86 functional and the atom-pairwise dispersion correction with Becke-Johnson damping scheme (D3BJ).[115-117] The resolution of the identity (RIJCOSX) approximation was used to accelerate the calculations in conjunction with appropriate basis sets (def2-TZVPP/J and def2-QZVP/J for the pnictogen atom, respectively).[118] Effective core potentials (ECP) for Sb and Bi were used as implemented in ORCA 4.0.[119,120] For interaction energies, the B3LYP functional was used instead of the BP86 functional and the resolution of the identity (RIJK) was used in an appropriate basis set (def2-TZVPP/JK and def2-QZVP/JK for the pnictogen atom, respectively) was used to speed up the calculations.[121-123] Natural bond orbital analysis was performed using the NBO 6.0 program.[124] Visualization of the NBO interaction was performed with GaussView 5.0.[125]

The bond dissociation energies were calculated with the Boys and Bernardi counterpoise correction (CP) to compensate the basis set superposition error (BSSE).[126-129] DLPNO-CCSD(T) calculations with LED have been carried out on the optimized Monomer structures and the monomer and dimer structures obtained from the crystal structure analysis DLPNO-CC calculations have been performed at the DLPNO-CCSD(T1) level of theory[73-78] using the cc-pVTZ basis set[130] and the cc-pVTZ-pp basis set for As, Sb and Bi with SK-MCDHF-RSC ECPs.[130] The RI approximation has been used throughout with the corresponding Aux basis sets[131] (and ORCAs Autoaux[132] sets if not otherwise available). Tight SCF convergence thresholds were applied, and the TightPNO settings for the DLPNO approximation were applied.[133]

Supporting Information

The Supporting Information is available free of charge on the ACS Publications website.
Experimental procedures, ^{1}H, ^{13}C NMR and IR spectra, crystallographic details, bond lengths and angles of **1** and **3**-**8** and results from quantum chemical calculations (pdf).

Corresponding Author

* Prof. Stephan Schulz, stephan.schulz@uni-due.de.

Notes

The authors declare no competing financial interests.

ACKNOWLEDGMENT

Financial support by the German Research Foundation within the priority program SPP 1807 "Control of London Dispersion Interactions in Molecular Chemistry" (S.S., A.A.) and the International Max Planck Research School (IMPRS Recharge, K.D.) is acknowledged. We also thank Prof. G. Jansen for valuable discussions.

REFERENCES

[1] For a historical review see: Seyferth, D. Cadet's Fuming Arsenical Liquid and the Cacodyl Compounds of Bunsen. *Organometallics* **2001**, *20*, 1488–1498.

[2] Paneth, F. A. The use of free methyl and ethyl in chemical synthesis. *Trans. Faraday Soc.* **1934**, *30*, 179–181.

[3] Paneth F. A.; Loleit, H. Free organic radicals in the gaseous state. Part IV. Synthesis of antimony cacodyl and related substances by the use of free methyl and free ethyl. *J. Chem. Soc.* **1935**, 366–371.

[4] Barrett A. G. M.; Melcher, L. M. Tetraphenyl distibine: a most useful reagent for discriminating radical reactions. *J. Am. Chem. Soc.* **1991**, *113*, 8177–8178.

[5] Ishida, S.; Hirakawa, F.; Furukawa, K.; Yoza, K.; Iwamoto, T. Persistent Antimony- and Bismuth-Centered Radicals in Solution. *Angew. Chem.* **2014**, *126*, 11354–11358; *Angew. Chem. Int. Ed.* **2014**, *53*, 11172–11176.

[6] Schwamm, R. J.; Harmer, J. R.; Lein, M.; Fitchett, C. M.; Granville S.; Coles, M. P. Isolation and Characterization of a Bismuth(II) Radical. *Angew. Chem.* **2015**, *127*, 10776–10779; *Angew. Chem. Int. Ed.* **2015**, *54*, 10630–10633.

[7] Zhao, M.-G.; Hao, T.-T.; Zhang, X.; Ma, J.-P.; Su, J.-H.; Zheng, W. Direct Evidence for Neutral *N*-Pyrazolyl Radicals: Paddlewheel Dibismuthanes Bearing Pyrazolato Ligands with Very Short Bi–Bi Single Bonds. *Inorg. Chem.* **2017**, *56*, 12678–12681.

[8] Ashe III, A. J.; Butler W.; Diephouse, T. R. 2,2',5,5'-Tetramethyldistibolyl. A thermochromic distibine. *J. Am. Chem. Soc.* **1981**, *103*, 207–209.

[9] Ashe III, A. J.; Ludwig Jr., E. G.; Oleksyszyn, J. Preparation and properties of dibismuthines. *Organometallics* **1983**, *2*, 1859–1866.

[10] Ashe III, A. J.; Ludwig Jr., E. G.; Oleksyszyn, J.; Huffman, J. C. The structure of tetramethyldistibine. *Organometallics* **1984**, *3*, 337–338.

[11] Roller, S.; Dräger, M.; Breunig, H. J.; Ates M.; Gülec, S. $(Me_3Sn)_2Sb$-$Sb(SnMe_3)_2$, $^1{}_\infty$-verknüpfte Sb-Sb-Hanteln in einem thermochromen Distiban mit Schweratomgerüst. *J. Organomet. Chem.* **1987**, *329*, 319–326.

[12] Mundt, O.; Riffel, H.; Becker G.; Simon, A. Element—Element-Bindungen, IV. Molekül- und Kristallstruktur des Tetramethyldiphosphans und -diarsans. *Z. Naturforsch. B* **1988**, *43*, 952–958.

[13] Becker, G.; Meiser, M.; Mundt, O.; Weidlein, J. Element–Element-Bindungen, V. Synthese, Molekül- und Kristallstruktur des Tetrakis(trimethylstannyl)distibans. *Z. Anorg. Allg. Chem.* **1989**, *569*, 62–82.

[14] Roller, S.; Dräger, M.; Breunig, H. J.; Ates M.; Gülec, S. Kristallstruktur, thermische Ausdehnung und Farbwechsel von $(Me_3Ge)_2Sb$-$Sb(GeMe_3)_2$ und anderen Distibanen. *J. Organomet. Chem.* **1989**, *378*, 327–337.

[15] Hughbanks, T.; Hoffmann, R.; Whangbo, M.-H.; Stewart, K. R.; Eisenstein, O.; Canadell, E. Electronic origin of the thermochromic effect in 2,2',5,5'-tetramethylbistibole. *J. Am. Chem. Soc.* **1982**, *104*, 3876–3879.

[16] Ashe III, A. J.; Kampf, J. W.; Puranik, D. B. Secondary bonding in organobismuth compounds. Comparison of the structures of 2,2',5,5'-tetramethyl-1,1'-dibismaferrocene and 2,2',5,5'-tetramethylbibismole. *Organometallics* **1992**, *11*, 2743–2745.

[17] Lohr, L. L.; Ashe III, A. J. Electronic structure of organobismuth compounds: effective core potential and semiempirical calculations. *Organometallics* **1993**, *12*, 343–346.

[18] Balázs, G.; Breunig, H. J.; Lork, E.; Offermann, W. Two Stable Hydrides of Antimony: $RSbH_2$ and R(H)Sb–Sb(H)R (R = $(Me_3Si)_2CH$). *Organometallics* **2001**, *20*, 2666–2668.

[19] Balázs, G.; Breunig, H. J.; Lork, E. Synthesis and Characterization of R_2SbH, R_2BiH, and $R_2Bi–BiR_2$ [R = $(Me_3Si)_2CH$]. *Organometallics* **2002**, *21*, 2584–2586.

[20] Hardman, N. J.; Twamley, B.; Power P. P. (2,6-$Mes_2H_3C_6)_2BiH$, a Stable, Molecular Hydride of a Main Group Element of the Sixth Period, and Its Conversion to the Dibismuthene (2,6-$Mes_2H_3C_6$)BiBi(2,6-$Mes_2C_6H_3$). *Angew. Chem. Int. Ed*. **2000**, *39*, 2771–2773.

[21] Balázs, L.; Breunig, H. J.; Lork, E.; Silvestru, C. Low-Valent Organobismuth Compounds with Intramolecular Coordination: *cyclo*-R_3Bi_3, *cyclo*-R_4Bi_4, RBi[W(CO)$_5$]$_2$, and R_4Bi_2 [R = 2-$(Me_2NCH_2)C_6H_4$]. *Eur. J. Inorg. Chem*. **2003**, 1361–1365.

[22] Balázs, L.; Breunig, H. J.; Lork, E. Synthesis and Crystal Structure of Tetramesityldibismuthane. *Z. Naturforsch. B* **2005**, *60*, 180–183.

[23] Balázs, L.; Breunig, H. J.; Silvestru, C.; Varga, R. Synthesis and Crystal Structure of *meso*-R(Ph)Sb-Sb(Ph)R [R = $(Me_3Si)_2CH$]. *Z. Naturforsch. B* **2005**, *60*, 1321–1324.

[24] Balázs, G.; Breunig, H. J.; Lork, E.; Soran, A.; Silvestru, C. Isomers of a Dibismuthane, $R_2Bi–BiR_2$ [R = 2,6-$(Me_2NCH_2)_2C_6H_3$], and Unusual Reactions with Oxygen: Formation of $[R_2Bi]_2(O_2)$ and R'R''Bi [R' = 2-(Me_2NCH_2)-6-{$Me_2N(O)CH_2$}C_6H_3; R'' = 2-(Me_2NCH_2)-6-{O(O)C}C_6H_3]. *Inorg. Chem*. **2006**, *45*, 2341–2346.

[25] Wolf, R.; Fischer, J.; Fischer, R. C.; Fettinger, J. C.; Power, P. P. Reactions of Terphenylbismuth Dihalides with $KSi(SiMe_3)_3$, $K_2Si_2(SiMe_3)_4$ and $Na_2[Fe(CO)]_4$: Reduction vs. Metathesis. *Eur. J. Inorg. Chem*. **2008**, 2515–2521.

[26] Breunig, H. J.; Lork, E.; Moldovan, O.; Rat, C. I. Syntheses of a stable tristibine and of related antimony compounds with the 2,6-dimesitylphenyl (Dmp) substituent. *J. Organomet. Chem*. **2008**, *693*, 2527–2534.

[27] Dostál, L.; Jambor, R.; Růžička, A.; Šimon, P. On the Reduction of NC Chelated Organoantimony(III) Chlorides. *Eur. J. Inorg. Chem*. **2011**, 2380–2386.

[28] Shimada, S.; Maruyama, J.; Choe, Y.-K.; Yamashita, T. A unique Bi–Bi bond forming reaction using organobismuth oxides and phosphorus compounds bearing a P(=O)H group. *Chem. Commun*. **2009**, 6168–6170.

[29] Monakhov, K. Y.; Zessin, T.; Linti, G. Reduction vs. Metathesis in the Reactions of Bismuth Tribromide with a Bulky Lithium Silanide – An Experimental and Theoretical Study. *Eur. J. Inorg. Chem*. **2010**, 322–332.

[30] Cambridge Structural Database, Version 5.40, see also: Allen, F. H. Applications of the Cambridge Structural Database in chemical education. *Acta Cryst.* **2002**, *B58*, 380-388. A search for the binuclear fragment "$C_4P_2M_2$" (M = any main group and transition metal) gave 88 hits, whereas the number of diarsine (6 hits), distibine (16 hits) and dibismuthine complexes (2 hits) is significantly lower.

[31] Schulz, S. Group 13/15 Organometallic Compounds - Synthesis, Structure, Reactivity and Potential Applications, *Adv. Organomet. Chem*. **2003**, *49*, 225–317.

[32] Kuczkowski, A.; Heimann, S.; Weber, A.; Schulz, S.; Bläser, D.; Wölper, C. Structural Characterization of Sb_2Et_4 and Bi_2Et_4. *Organometallics* **2011**, *30,* 4730–4735.

[33] Schulz, S.; Heimann, S.; Kuczkowski, A.; Wölper, C.; Bläser, D. The Origin of Thermochromic Behaviour in Distibines - Still an open Question. *Organometallics* **2013**, *32*, 3391–3394.

[34] Kuczkowski, A.; Fahrenholz, S.; Schulz, S.; Nieger, M.; Saarenketo, P. Reactivity of Distibanes towards Trialkylalanes and -gallanes - Syntheses and X-Ray Structures of Bisadducts and Heterocycles. *Organometallics* **2001**, *20*, 2000–2006.

[35] Kuczkowski, A.; Schulz, S.; Nieger, M. Reactions of Et_4Bi_2 with *t*-Bu_3M (M = Al, Ga) - Synthesis of complexes with a bidentate dibismuthine ligand. *Angew. Chem*. **2001**, *113*, 4351–4353; *Angew. Chem. Int. Ed*. **2001**, *40*, 4222–4225.

[36] Kuczkowski, A.; Fahrenholz, S.; Schulz, S.; Nieger, M. Reactions of Distibines Sb_2R_4 and Dibismuthine Bi_2Et_4 with Trialkyltrieles MR_3. *Organometallics* **2004**, *23*, 3615–3621.

[37] Schuchmann, D.; Kuczkowski, A.; Fahrenholz, S.; Schulz, S.; Flörke, U. Reactions of Group 13 Organometallics *t*-Bu_3M with Distibanes Sb_2R_4. *Eur. J. Inorg. Chem*. **2007**, 931–935.

[38] Ganesamoorthy, C.; Bläser, D.; Wölper, C.; Schulz, S. Temperature-Dependent Electron Shuffle in Molecular Group 13/15 Intermetallic Complexes. *Angew. Chem*. **2014**, *126*, 11771–11775; *Angew. Chem. Int. Ed*. **2014**, *53*, 11587–11591.

[39] Heimann, S.; Schulz, S.; Bläser, D.; Wölper, C. Syntheses and Solid State Structures of Bis(dialkylstibanyl) Sulfanes and Telluranes. *Eur. J. Inorg. Chem*. **2013**, *28*, 4909–4915.

[40] Heimann, S.; Kuczkowski, A.; Bläser, D.; Wölper, C.; Haack, R.; Jansen, G.; Schulz, S. Syntheses and Solid State Structures of $Et_2SbTeEt$ and $Et_2BiTeEt$. *Eur. J. Inorg. Chem*. **2014**, *28*, 4858–4864.

[41] Heimann, S.; Bläser, D.; Wölper, C.; Schulz, S. Solid-State Structures of Bis(diethylbismuthanyl)sulfane, -selenane, and -tellurane. *Organometallics* **2014**, *33*, 2295–2300.

[42] Karacar, A.; Thonnessen, H.; Jones, P. G.; Bartsch, R.; Schmutzler, R. 1,8-Bis(phosphanyl)naphthalenes: 1,8-Bis[(diethylamino)phosphanyl]-naphthalene, 1,8-Bis(dichlorophosphany)naphthalene, and 1, 3-Dichloro-2,-3-dihydro-1,3-dioxo-2-oxa-1,3-diphosphaphenalene. *Chem. Ber./Recueil* **1997**, *130*, 1485–1489.

[43] Karacar, A.; Freytag, M.; Thonnessen, H.; Jones, P. G.; Bartsch, R.; Schmutzler, R. Preparation and structures of 1-dimethylamino-2-bis(dimethylamino)- and 1-chloro-2-bis(diethylamino)-1-phospha-2-phosphonium acenaphthene: the first examples of the 1,2-dihydro-1,2-diphospha-acenaphthene ring system. *J. Organomet. Chem*. **2002**, *643–644*, 68–80.

[44] Kilian, P.; Slawin, A. M. Z.; Woollins, J. D. Naphthalene-1,8-diyl Bis(Halogenophosphanes): Novel Syntheses and Structures of Useful Synthetic Building Blocks. *Chem. Eur. J*. **2003**, *9*, 215–222.

[45] Owsianik, K.; Vendier, L.; Błaszczyk, J.; Sieroń, L. Synthesis and structures of non-cyclic and cyclic mono- and bisphosphonium salts derived from 1,8-bis(diphenylphosphino)naphthalene. *Tetrahedron* **2013**, *69*, 1628–1633.

[46] Taylor, L. J.; Bühl, M.; Chalmers, B. A.; Ray, M. J.; Wawrzyniak, P.; Walton, J. C.; Cordes, D. B.; Slawin, A. M. Z.; Woollins, J. D.; Kilian, P. Dealkanative Main Group Couplings across the peri-Gap. *J. Am. Chem. Soc*. **2017**, *139*, 18545–18551.

[47] Jura, M.; Levason, W.; Reid, G.; Webster, M. Preparation and properties of sterically demanding and chiral distibine ligands. *Dalton Trans*. **2008**, 5774–5782.

[48] Aucott, S. M.; Milton, H. L.; Robertson, S. D.; Slawin, A. M. Z.; Woollins, J. D. Crystal structures and molecular modeling of 1,8 chalcogenide-substituted naphthalenes. *Heteroatom Chem*. **2004**, *15*, 530–542.

[49] Knight, F. R.; Fuller, A. L.; Bühl, M.; Slawin, A. M. Z.; Woollins, J. D. Synthetic and Structural Studies of 1-Halo-8-(alkylchalcogeno)naphthalene Derivatives. *Chem. Eur. J.* **2010**, *16*, 7605–7616.

[50] Knight, F. R.; Fuller, A. L.; Bühl, M.; Slawin A. M. Z., Woollins, J. D. Synthetic and Structural Studies of 1,8-Chalcogen Naphthalene Derivatives. *Chem. Eur. J*. **2010**, *16*, 7503–7516.

[51] Wang, W.; Sun, Z.; Meng, L.; Li, X. Intriguing E…E' bonding in $[Nap(EPh)(E'Ph)]^{\bullet+}$ (E, E'=O, S, Se, Te). *Int. J. Quant. Chem.* **2016**, *116*, 1090–1096.

[52] Wohltmann, W.; Mostaghimi, F.; Bolsinger, J.; Lork, E.; Mebs, S.; Beckmann, J. Synthesis and halogenation of bis(8-methoxynaphthyl)ditelluride. *Inorg. Chim. Acta* **2018**, *475*, 73–82.

[53] Knight, F. R.; Fuller, A. L.; Bühl, M.; Slawin, A. M. Z.; Woollins, J. D. Sterically Crowded *peri*-Substituted Naphthalene Phosphines and their P^V Derivatives. *Chem. Eur. J*. **2010**, *16*, 7617–7634.

[54] Kirst, C.; Bode, B. E.; Cordes, D. B.; Nejman, P. S.; Slawin, A. M. Z.; Karaghiosoff, K.; Woollins, J. D. Diphosphane 2,2′-binaphtho[1,8-de][1,3,2]dithiaphosphinine and the easy formation of a

stable phosphorus radical cation. *Dalton Trans.* **2016**, *45*, 6348–6351.

[55] Kilian, P.; Knight, F. R.; Woollins, J. D. Naphthalene and Related Systems *peri*-Substituted by Group 15 and 16 Elements. *Chem. Eur. J.* **2011**, *17*, 2302–3228.

[56] Kilian, P.; Knight, F. R.; Woollins, J. D. Synthesis of ligands based on naphthalene *peri*-substituted by Group 15 and 16 elements and their coordination chemistry. *Coord. Chem. Rev.* **2011**, *255*, 1387–1413.

[57] Ganesamoorthy, C.; Heimann, S.; Hölscher, S.; Haack, R.; Wölper, C.; Jansen, G.; Schulz, S. Synthesis, structure and dispersion interactions in bis(1,8-naphthalendiyl)distibine. *Dalton Trans.* **2017**, *46*, 9227–9234.

[58] Mizuta, T.; Nakazono, T.; Miyoshi, K. Naphtho[1,8-*b*,*c*]phosphete and 1,2-Diphosphaacenaphthene from the Reaction of 1,8-Dilithionaphthalene with $RPCl_2$. *Angew. Chem.* **2002**, *114*, 4053–4054; *Angew. Chem. Int. Ed.* **2002**, *41*, 3897–3898.

[59] Baba, M.; Mizuta, T. Synthesis of bicyclic diphosphine having a P–P bond doubly clamped with two 1,8-naphthalenediyl groups. *Polyhedron* **2015**, *92*, 30–36.

[60] Wagner, J. P.; Schreiner, P. R. London Dispersion Decisively Contributes to the Thermodynamic Stability of Bulky NHC-Coordinated Main Group Compounds. *J. Chem. Theory Comput.* **2016**, *12*, 231-237.

[61] Wagner, J. P.; Schreiner, P. R. London Dispersion in Molecular Chemistry—Reconsidering Steric Effects. *Angew. Chem. Int. Ed.* **2015**, *54*, 12274-12296.

[62] Liptrot, D. J.; Power, P. P. London dispersion forces in sterically crowded inorganic and organometallic molecules. *Nat. Rev. Chem.* **2017**, *1*, 0004.

[63] Auer, A. A.; Mansfeld, D.; Nolde, C.; Schneider, W.; Schürmann, M.; Mehring, M. Bismuth–Arene π-Interaction: A Combined Experimental and Theoretical Approach. *Organometallics* **2009**, *28*, 5405–5411.

[64] Schmidbaur, H.; Schier, A. π-Complexation of Post-Transition Metals by Neutral Aromatic Hydrocarbons: The Road from Observations in the 19th Century to New Aspects of Supramolecular Chemistry. *Organometallics* **2008**, *27*, 2361–2395.

[65] Silvestru, C.; Breunig, H. J.; Althaus, H. Structural Chemistry of Bismuth Compounds. I. Organobismuth Derivatives. *Chem. Rev.* **1999**, *99*, 3277–3328.

[66] Cangelosi, V. M.; Pitt, M. A.; Vickaryous, W. J.; Allen, C. A.; Zakharov, L. N.; Johnson, D. W. Design Considerations for the Group 15 Elements: The Pnictogen⋯π Interaction As a Complementary Component in Supramolecular Assembly Design. *Cryst. Growth Des.* **2010**, *10*, 3531–3536.

[67] Zukerman-Schpector, J.; Tiekink, E. R. T. Intermolecular C–H⋯π(Chelate) Interactions – Prevalence in the Crystal Structures of Metal 1,1-Dithiolates. In The Importance of Pi-Interactions in Crystal Engineering, John Wiley & Sons, Chichester, U.K., **2012**; pp 275–299.

[68] Krasowska, M.; Schneider, W. B.; Mehring, M.; Auer, A. A. High-Level Ab Initio Calculations of Intermolecular Interactions: Heavy Main-Group Element pi-Interactions. *Chem. Eur. J.* **2018**, *24*, 10238–10245.

[69] Song, L.; Schoening, J.; Wölper, C.; Schulz, S.; Schreiner P. R. The Role of London Dispersion Interactions in Ga-Substituted Dipnictenes. *Organometallics* **2019**, *38*, 1640–1647.

[70] Haack, R.; Schulz S.; Jansen G. Dispersion interactions between neighboring Bi atoms in $(BiH_3)_2$ and $Te(BiR_2)_2$. *J. Comput. Chem.* **2018**, *39*, 1413–1423.

[71] Cambridge Structural Database, Version 5.40, see also: Allen, F. H. Applications of the Cambridge Structural Database in chemical education. *Acta Cryst.* **2002**, *B58*, 380–388. Search for $X_2As\text{-}AsX_2$ (As with c.n. 3 and acyclic; X = any atom) gave 25 hits. As-As bond ranges from 2.417 - 2.592 Å (mean deviation 0.054 Å).

[72] Cordero, B.; Gómez, V.; Platero-Prats, A. E.; Revés, M.; Echeverría, J.; Cremades, E.; Barragán, F.; Alvarez, S. Covalent radii revisited. *Dalton Trans.* **2008**, 2832–2838.

[73] F. Neese, A. Hansen, D. G. Liakos, Efficient and accurate approximations to the local coupled cluster singles doubles method using a truncated pair natural orbital basis, *J. Chem. Phys.* **2009**, *131*, 064103-1–15.

[74] D. G. Liakos, A. Hansen, F. Neese, Weak Molecular Interactions Studied with Parallel Implementations of the Local Pair Natural Orbital Coupled Pair and Coupled Cluster Methods, *J. Chem. Theory Comput.* **2011**, *7*, 76–87.

[75] C. Riplinger, F. Neese, An efficient and near linear scaling pair natural orbital based local coupled cluster method, *J. Chem. Phys.* **2013**, *138*, 034106-1–18.

[76] C. Riplinger, B. Sandhoefer, A. Hansen, F. Neese, Natural triple excitations in local coupled cluster calculations with pair natural orbitals, *J. Chem. Phys.* **2013**, *139*, 134101-1–13.

[77] C. Riplinger, P. Pinski, U. Becker, E. F. Valeev, F. Neese, Sparse maps—A systematic infrastructure for reduced-scaling electronic structure methods. II. Linear scaling domain based pair natural orbital coupled cluster theory, *J. Chem. Phys.* **2016**, *144*, 024109-1–10.

[78] Y. Guo, C. Riplinger, U. Becker, D. G. Liakos, Y. Minenkov, L. Cavallo, F. Neese, Communication: An improved linear scaling perturbative triples correction for the domain based local pair-natural orbital based singles and doubles coupled cluster method [DLPNO-CCSD(T)], *J. Chem. Phys.* **2018**, *148*, 011101-1–5.

[79] G. Bistoni, A. A. Auer, F. Neese, Understanding the Role of Dispersion in Frustrated Lewis Pairs and Classical Lewis Adducts: A Domain-Based Local Pair Natural Orbital Coupled Cluster Study, *Chem. Eur. J.* **2017**, *23*, 865–873.

[80] A. Altun, F. Neese, G. Bistoni, Effect of Electron Correlation on Intermolecular Interactions: A Pair Natural Orbitals Coupled Cluster Based Local Energy Decomposition Study, *J. Chem. Theory Comput.* **2019**, *15*, 215–228.]

[81] Mantina, M.; Chamberlin, A. C.; Valero, R.; Cramer, C. J.; Truhlar, D. G. Consistent van der Waals Radii for the Whole Main Group. *J. Phys. Chem. A* **2009**, *113*, 5806–5812.

[82] Vránová, I.; Kremláček, V.; Erben, M.; Turek, J.; Jambor, R.; Růžička, A.; Alonso, M.; Dostál L. A comparative study of the structure and bonding in heavier pnictinidene complexes [(ArE)M(CO)n] (E = As, Sb and Bi; M = Cr, Mo, W and Fe). *Dalton Trans.* **2017**, *46*, 3556-3368.

[83] Fischer, E. O.; Bathelt, W.; Müller, J. Stibin-pentacarbonyl-Komplexe von Chrom(O), Molybdan(0) und Wolfram(0). *Chem. Ber.* **1971**, *104*, 986-992.

[84] Davies, M. S.; Allen, G. W.; Aroney, M. J. Conformational studies of $EPh_3M(CO)_5$ complexes (E = P, As or Sb; M = Cr, Mo, or W). *J. Mol. Struct.* **1994**, *326*, 81-91.

[85] Delbeke, F. T.; Van der Kelen, G. P. Transition metal chemistry: VIII. Synthesis and IR study of monosubstitution products of $Cr(CO)_6$ and tertiary substituted aryl group VB derivatives. *J. Organomet. Chem.* **1974**, *64*, 239-244.

[86] Aroney, M. J.; Clarkson, R. M.; Hambley, T. W.; Pierens, R. K. A study of polarities, polarisabilities and infrared spectra of LM(CO), complexes (M = Cr, MO or W; L = trimethylamine, quinuclidine, pyridine, p-methyl- or p-t-butylpyridine) and of the X-ray crystal structure of quinuclidine-Cr(CO): evidence for acceptor behaviour of coordinated pyridine. *J. Organomet. Chem.* **1992**, *426*, 331-342.

[87] Davies, M. S.; Pierens, R. K.; Aroney, M. J. Metal—ligand bonding in $LM(CO)_5$ complexes (L = NMe_3, PMe_3, PCl_3, PBr_3 or $AsMe_3$; M = Cr, Mo or W) from dielectric, electro-optic and spectroscopic evidence. *J. Organomet. Chem.* **1993**, *458*, 141-146..

[88] Shufler, S. L.; Sternberg, H. W.; Friedel, R. A. Infrared Spectrum and Structure of Chromium Hexacarbonyl, $Cr(CO)_6$, *J. Am. Chem. Soc.* **1956**, *78*, 2687–2688.

[89] Orgel L. E. The Infrared Spectra of Substituted Metal Carbonyls. *Inorg. Chem.* **1962**, *1*, 25 -29.

[90] Weber, L.; Meyer, M.; Stammler, H. G.; Neumann, B. Reactivity of the Inversely Polarized Phosphaalkenes $RP{=}C(NMe_2)_2$ (R = *t*Bu, Me_3Si, H) towards Arylcarbene Complexes $[(CO)_5M{=}C(OEt)Ar]$

(Ar = Ph, M = Cr, W; Ar = 2-MeC_6H_4, 2-$MeOC_6H_4$, M = W). *Chem. Eur. J.* **2001**, *7*, 5401–5408.

[91] Bockfeld, D.; Doddi, A.; Jones, P. G.; Tamm, M. Transition-Metal Carbonyl Complexes and Electron-Donating Properties of N-Heterocyclic-Carbene–Phosphinidene Adducts. *Eur. J. Inorg. Chem.* **2016**, 3704–3712.

[92] Cowley, A. H.; Lasch, J. G.; Norman, N. C.; Pakulski M. Synthesis and Structure of a Diarsenechromium Complex with an Unsupported Arsenic-Arsenic Double Bond. *Angew. Chem. Int. Ed.* **1983**, *22*, 978–979.

[93] Kuczkowski, A.; Schulz, S.; Nieger, M.; Saarenketo, P. Reactivity of Distibanes towards Trialkylalanes and -gallanes - Syntheses and X-Ray Structures of Bisadducts and Heterocycles. *Organometallics* **2001**, *20*, 2000–2006.

[94] Schuchmann, D.; Kuczkowski, A.; Fahrenholz, S.; Schulz, S.; Flörke, U. Reactions of Group 13 Organometallics *t*-Bu_3M with Distibines Sb_2R_4. *Eur. J. Inorg. Chem.* **2007**, 931–935.

[95] Becker, G.; Freudenkamp, H.; Witthauer, C. Synthese, Molekül- und Kristallstruktur des Tetrakis(trimethylsilyl)distibans im Vergleich mit Tetraphenyldistiban. *Z. Anorg. Allg. Chem.* **1982**, *492*, 37–51.

[96] Lorenz, I.-P.; Rudolph, S.; Piotrowski, H.; Polborn, K. Reactions of $K_2[Fe(CO)_3(PPh_3)]$: Reductive Sb–Sb Coupling with Ph_2SbCl To Form *trans*-$[Fe(CO)_3(PPh_3)(Sb_2Ph_4)]$ and Salt Metathesis with Me_3SbCl_2 To Yield *trans*-$[Fe(CO)_3(PPh_3)(SbMe_3)]$. *Eur. J. Inorg. Chem.* **2005**, 82–85.

[97] Breunig, H. J.; Ghesner, I.; Ghesner, M. E.; Lork, E. Syntheses and coordination chemistry of di-, tri-, and tetrastibanes, $R_2Sb(SbR')_nSbR_2$ (n=0, 1, 2). *J. Organomet. Chem.* **2003**, *677*, 15–20.

[98] Mundt, O.; Riffel, H.; Becker, G.; Simon, A. Element–Element-Bindungen III, Intermolekulare Sb-Sb-Wechsel Wirkungen im kristallinen Tetramethyldistiban. *Z. Naturforsch. B* **1984**, *39*, 317–322.

[99] von Seyerl, J.; Huttner, G. Bis-pentacarbonylchromium-tetraphenyldistibane $C_{34}H_{20}Cr_2O_{10}Sb_2$. *Cryst. Struct. Comm.* **1980**, *9*, 1099–1103.

[100] Breunig, H. J.; Ghesner, I.; Ghesner, M. E.; Lork, E. Syntheses and coordination chemistry of di-, tri-, and tetrastibanes, $R_2Sb(SbR')_nSbR_2$ (n=0, 1, 2). *J. Organomet. Chem.* **2003**, *677*, 15–20.

[101] Weber, U.; Zsolnai, L.; Huttner, G. Synthesen und Strukturen von Distibankomplexen. *Z. Naturforsch. B* **1985**, *40*, 1430–1436.

[102] Teramoto, Y.; Kubo, K.; Mizuta, T. PhP–PPh group bound to 1,8-positions of naphthalene: Preparation of cis isomer and synthesis of binuclear complex. *J. Organomet. Chem.* **2011**, *696*, 3402–3407.

[103] Twamley, B.; Sofield, C. D.; Olmstead, M. M.; Power, P. P. Homologous Series of Heavier Element Dipnictenes 2,6-$Ar_2H_3C_6E)EC_6H_3$-2,6-Ar_2 (E = P, As, Sb, Bi; Ar = Mes = C_6H_2-2,4,6-Me_3; or Trip = C_6H_2-2,4,6-$^iPr_3$) Stabilized by m-Terphenyl Ligands *J. Am. Chem. Soc.* **1999**, *121*, 3357–3367.

[104] Vickaryous, W. J.; Herges, R.; Johnson, D. W. Arsenic–π Interactions Stabilize a Self-Assembled As_2L_3 Supramolecular Complex, *Angew. Chem. Int. Ed.* **2004**, *43*, 5831–5833.

[105] Wuttke, A.; Mata, R. A. Visualizing dispersion interactions through the use of local orbital spaces. *J. Comput. Chem.* **2017**, *38*, 15–23.

[106] Schmidbaur, H.; Nowak, R.; Huber, B.; Müller G. Hexaethylbenzene-Trichloroantimony: A Menshutkin Complex with a Centroid Antimony-Arene Coordination. *Organometallics* **1987**, *6*, 2266–2267.

[107] Mootz, D.; Händler, V. Crystal Structure of the Menshutkin Complex Benzene·$2SbCl_3$ *Z. Anorg. Allg. Chem.* **1986**, *533*, 23–29.

[108] Lo, R.; Švec, P.; Růžičková, Z.; Růžička, A.; Hobza, P. On the nature of the stabilisation of the E⋯π pnicogen bond in the $SbCl_3$⋯toluene complex, *Chem. Commun.* **2016**, *52*, 3500–3503.

[109] Caracelli, I.; Haiduc, I.; Zukerman-Schpector, J.; Tiekink, E. R. T. Delocalised antimony(lonepair)- and bismuth-(lonepair)⋯π(arene) interactions: Supramolecular assembly and other considerations, *Coord. Chem. Rev.* **2013**, *257*, 2863–2879.

[110] Weber, L.; Bungardt, D.; Boese, R. Übergangsmetall-funktionalisierte Phosphaarsene als Liganden in Pentacarbonylchrom-Komplexen. Röntgenstrukturanalyse von $(\eta^5\text{-}C_5Me_5)(CO)_2Fe$–$As[Cr(CO)_5]$=P–$C_6H_2$(*t*-Bu)$_3$(2,4,6). *Chem. Ber.* **1988**, *121*, 1535–1539.

[111] Sheldrick, G. Phase annealing in SHELX-90: direct methods for larger structures. *Acta Crystallogr.* **1990,** *A46*, 467–473.

[112] Sheldrick, G. A short history of SHELX. *Acta Crystallogr.* **2008,** *A64*, 112–122.

[113] Hübschle, C. B.; Sheldrick, G. M.; Dittrich, B. ShelXle: a Qt graphical user interface for SHELXL. *J. Appl. Crystallogr.* **2011,** *44*, 1281–1284.

[114] Neese, F. The ORCA program system, *WIREs Comput Mol Sci* **2012**, *2*, 73–78.

[115] Perdew, J. P.; Yue, W. Accurate and simple density functional for the electronic exchange energy: Generalized gradient approximation. *Phys. Rev. B* **1986**, *33*, 8800–8802.

[116] Perdew, J. P.; Yue, W. Erratum: Accurate and simple density functional for the electronic exchange energy: Generalized gradient approximation. *Phys. Rev. B* **1989**, *40*, 3399.

[117] Grimme, S.; Ehrlich, S.; Goerigk, L. *J.* Effect of the damping function in dispersion corrected density functional theory. *Comput. Chem.* **2011**, *32*, 1456–1465.

[118] Weigend, F. Accurate Coulomb-fitting basis sets for H to Rn. *Phys. Chem. Chem. Phys.* **2006**, *8*, 1057–1065.

[119] Leininger, T.; Nicklass, A.; Küchle, W.; Stoll, H.; Dolg, M.; Bergner, A. The accuracy of the pseudopotential approximation: non-frozen-core effects for spectroscopic constants of alkali fluorides XF (X = K, Rb, Cs). *Chem. Phys. Lett.* **1996**, *255*, 274–280.

[120] Metz, B.; Stoll, H.; Dolg, M. Small-core multiconfiguration-Dirac–Hartree–Fock-adjusted pseudopotentials for post-d main group elements: Application to PbH and PbO. *J. Chem. Phys.* **2000**, *113*, 2563–2569.

[121] Weigend, F. Accurate Coulomb-fitting basis sets for H to Rn. *Phys. Chem. Chem. Phys.* **2006**, *8*, 1057–1065.

[122] Lee, C.; Yang, W.; Parr, R. G. Development of the Colle-Salvetti correlation-energy formula into a functional of the electron density. *Phys. Rev. B* **1988**, *37*, 785–789.

[123] Becke, A. D. Density-functional thermochemistry. III. The role of exact exchange. *J. Chem. Phys.* **1993**, *98*, 5648–5652.

[124] Glendening, E. D.; Landis, C. R.; Weinhold, F. NBO 6.0: Natural bond orbital analysis program. *J. Comput. Chem.* **2013**, *34*, 1429–1437.

[125] Frisch, E.; Hratchian, H. P.; Dennington II, R. D.; Keith, T. A.; Millam, J. A.; Nielsen, B. A.; Holder, J.; Hiscocks, J. GaussView 5 Reference, *Gaussian, Inc.*, Wallingford, CT, **2009**.

[126] Boys, S. F.; Bernardi, F. The calculation of small molecular interactions by the differences of separate total energies. Some procedures with reduced errors. *Mol. Phys.* **1970**, *19*, 553–566.

[127] Liu, B.; McLean, A. D. Accurate calculation of the attractive interaction of two ground state helium atoms. *J. Chem. Phys.* **1973**, *59*, 4557–4558.

[128] Asturiol, D.; Duran, M.; Salvador, P. Intramolecular basis set superposition error effects on the planarity of benzene and other aromatic molecules: A solution to the problem. *J. Chem. Phys.* **2008**, *128*, 144108.

[129] van Duijneveldt, F. B.; van Duijneveldt-van de Rijdt, J. G. C. M.; van Lenthe, J. H. State of the Art in Counterpoise Theory. *Chem. Rev.* **1994**, *94*, 1873–1885.

[130] Martin, J. M. L; Sundermann, A. Correlation consistent valence basis sets for use with the Stuttgart-Dresden-Bonn relativistic effective core potentials: the atoms Ga–Kr and In-Xe. *J. Chem. Phys.* **2001**, *8*, 3408–3420.

[131] Neese, F. An Improvement of the Resolution of the Identity Approximation for the Calculation of the Coulomb Matrix, *J. Comp. Chem.* **2003**, *24*, 1740–1747.

[132] Stoychev, G. L.; Auer, A. A.; Neese, F. Automatic Generation of Auxiliary Basis Sets. *J. Chem. Theory Comput.* **2017**, *13*, 554–562.

[133] Liakos, D. G.; Sparta, M.; Kesharwani, M. K.; Martin, J. M. L.; Neese, F. Exploring the Accuracy Limits of Local Pair Natural Orbital Coupled-Cluster Theory. *J. Chem. Theory Comput.* **2015**, *11*, 1525–1539.

We report on the structure of $Naph_2As_2$ **1** (Naph = 1,8-naphthalenediyl) and the σ-donor and redox activity of $Naph_2E_2$ (E = As **1**, Sb **2**). The occurrence of intermolecular As···π and Sb···π interactions is discussed and quantified by density functional theory and local coupled cluster electronic structure theory calculation, demonstrating how dispersion interactions change with the electronic structure of the compounds.

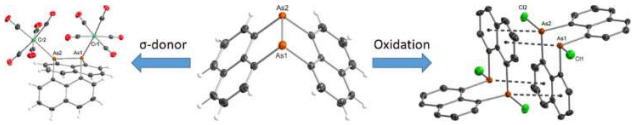

DOI: 10.1021/acs.organomet.9b00269
URN: urn:nbn:de:hbz:464-20210127-150143-5